

# Simple accurate mathematical models of blood HbO<sub>2</sub> and HbCO<sub>2</sub> dissociation curves at varied physiological conditions: evaluation and comparison with other models

Ranjan K. Dash<sup>1</sup> · Ben Korman<sup>2</sup> · James B. Bassingthwaight<sup>3</sup>

Received: 20 May 2015 / Accepted: 22 July 2015 / Published online: 23 August 2015  
© Springer-Verlag Berlin Heidelberg 2015

## Abstract

**Purpose** Equations for blood oxyhemoglobin (HbO<sub>2</sub>) and carbaminohemoglobin (HbCO<sub>2</sub>) dissociation curves that incorporate nonlinear biochemical interactions of oxygen and carbon dioxide with hemoglobin (Hb), covering a wide range of physiological conditions, are crucial for a number of practical applications. These include the development of physiologically-based computational models of alveolar-blood and blood-tissue O<sub>2</sub>–CO<sub>2</sub> transport, exchange, and metabolism, and the analysis of clinical and in vitro data.

**Methods and results** To this end, we have revisited, simplified, and extended our previous models of blood HbO<sub>2</sub> and HbCO<sub>2</sub> dissociation curves (Dash and Bassingthwaight, Ann Biomed Eng 38:1683–1701, 2010), validated wherever possible by available experimental data, so that the models now accurately fit the low HbO<sub>2</sub> saturation ( $S_{\text{HbO}_2}$ ) range over a wide range of values of  $P_{\text{CO}_2}$ , pH, 2,3-DPG, and temperature. Our new equations incorporate a novel

$P_{\text{O}_2}$ -dependent variable cooperativity hypothesis for the binding of O<sub>2</sub> to Hb, and a new equation for  $P_{50}$  of O<sub>2</sub> that provides accurate shifts in the HbO<sub>2</sub> and HbCO<sub>2</sub> dissociation curves over a wide range of physiological conditions. The accuracy and efficiency of these equations in computing  $P_{\text{O}_2}$  and  $P_{\text{CO}_2}$  from the  $S_{\text{HbO}_2}$  and  $S_{\text{HbCO}_2}$  levels using simple iterative numerical schemes that give rapid convergence is a significant advantage over alternative  $S_{\text{HbO}_2}$  and  $S_{\text{HbCO}_2}$  models.

**Conclusion** The new  $S_{\text{HbO}_2}$  and  $S_{\text{HbCO}_2}$  models have significant computational modeling implications as they provide high accuracy under non-physiological conditions, such as ischemia and reperfusion, extremes in gas concentrations, high altitudes, and extreme temperatures.

**Keywords** O<sub>2</sub> and CO<sub>2</sub> binding to hemoglobin · O<sub>2</sub> and CO<sub>2</sub> saturation of hemoglobin · Oxyhemoglobin and carbaminohemoglobin dissociation curves · Nonlinear O<sub>2</sub>–CO<sub>2</sub> interactions · Bohr and Haldane effects · Mathematical modeling

Communicated by Carsten Lundby.

✉ Ranjan K. Dash  
rdash@mcw.edu

✉ James B. Bassingthwaight  
jbb2@u.washington.edu

Ben Korman  
ben@korman.com.au

<sup>1</sup> Department of Physiology, Biotechnology and Bioengineering Center, Medical College of Wisconsin, 8701 Watertown Plank Road, Milwaukee, WI 53226, USA

<sup>2</sup> Department of Anaesthesia and Pain Medicine, Royal Perth Hospital, Perth, WA, Australia

<sup>3</sup> Department of Bioengineering, University of Washington, Box 355061, N210G North Foege Bldg, Seattle, WA 9895-5061, USA

## Abbreviations

|                        |   |
|------------------------|---|
| $\alpha_{\text{O}_2}$  | Solubility of oxygen in water                                   |
| $\alpha_{\text{CO}_2}$ | Solubility of carbon dioxide in water                           |
| [O <sub>2</sub> ]      | Concentration of free oxygen                                    |
| [CO <sub>2</sub> ]     | Concentration of free carbon dioxide                            |
| [H <sup>+</sup> ]      | Concentration of hydrogen ions (protons)                        |
| [DPG]                  | Concentration of 2,3-diphosphoglycerate (2,3-DPG)               |
| $T$                    | Temperature   |
| pH                     | $-\log_{10}([\text{H}^+])$                                      |
| $P_{\text{O}_2}$       | Partial pressure of oxygen                                      |
| $P_{\text{CO}_2}$      | Partial pressure of carbon dioxide                              |
| $P_{50}$               | Partial pressure of oxygen for 50 % HbO <sub>2</sub> saturation |

|                     |   |
|---------------------|---|
| Hb                  | Hemoglobin  |
| HbO <sub>2</sub>    | Oxyhemoglobin   |
| HbCO <sub>2</sub>   | Carbaminohemoglobin   |
| $K_{\text{HbO}_2}$  | Apparent equilibrium constant for the binding of oxygen to hemoglobin         |
| $K_{\text{HbCO}_2}$ | Apparent equilibrium constant for the binding of carbon dioxide to hemoglobin |
| $S_{\text{HbO}_2}$  | Saturation of hemoglobin with oxygen  |
| $S_{\text{HbCO}_2}$ | Saturation of hemoglobin with carbon dioxide                                  |

## Introduction

The delivery of oxygen to tissues for metabolism and energy production in parenchymal cells is regulated by a complex system of physicochemical processes in the microcirculation (Dash and Bassingthwaight 2006; Bassingthwaight et al. 2012). In systemic capillaries, the release of oxygen from hemoglobin (Hb) inside red blood cells (RBCs) depends in part on the simultaneous release of carbon dioxide into the flowing blood. In the lungs, the loss of CO<sub>2</sub> from RBCs increases O<sub>2</sub> uptake, which in turn enhances CO<sub>2</sub> dissociation from Hb. This interacting process also depends on the buffering of CO<sub>2</sub> by bicarbonate ions (HCO<sub>3</sub><sup>-</sup>), acid–base regulation, and the Hb-mediated nonlinear biochemical O<sub>2</sub>–CO<sub>2</sub> interactions inside RBCs (Geers and Gros 2000; Rees and Andreassen 2005; Dash and Bassingthwaight 2006; Bassingthwaight et al. 2012). In this regard, a decrease in pH or an increase in CO<sub>2</sub> partial pressure ( $P_{\text{CO}_2}$ ) in systemic capillaries decreases the affinity of O<sub>2</sub> for Hb and HbO<sub>2</sub> saturation ( $S_{\text{HbO}_2}$ ), and increases the delivery of O<sub>2</sub> to peripheral tissues (the Bohr effect). On the other hand, an increase in O<sub>2</sub> partial pressure ( $P_{\text{O}_2}$ ) in pulmonary capillaries results in the release of hydrogen ions (H<sup>+</sup>) from Hb, which in turn decreases the affinity of Hb for CO<sub>2</sub>, reducing HbCO<sub>2</sub> saturation ( $S_{\text{HbCO}_2}$ ) and aiding elimination of CO<sub>2</sub> by the lungs (the Haldane effect). Thus, both the Bohr and Haldane effects are important in defining the Hb-mediated nonlinear biochemical O<sub>2</sub>–CO<sub>2</sub> interactions inside RBCs (Siggaard-Andersen and Garby 1973; Tyuma 1984; Matejak et al. 2015). Raising blood temperature ( $T$ ) also lowers the affinity of O<sub>2</sub> for Hb, and increases the delivery of O<sub>2</sub> to tissues. Consequently, the integrated computational modeling of O<sub>2</sub> transport, exchange and metabolism in tissue-organ systems must account for the coupled transport and exchange of CO<sub>2</sub>, HCO<sub>3</sub><sup>-</sup>, H<sup>+</sup>, and heat in the microcirculation (Dash and Bassingthwaight 2006). This is particularly important in highly metabolic tissue-organ systems such as heart and skeletal muscle during exercise (von Restorff et al. 1977), where arteriovenous (AV) temperature increases of 1 °C or so,  $P_{\text{CO}_2}$  increases of nearly

10 mmHg, and pH decreases of about 0.1 pH unit, all combine to push the HbO<sub>2</sub> dissociation curve to the right. Under these conditions,  $P_{\text{O}_2}$  may decrease by as much as 80 mmHg and  $S_{\text{HbO}_2}$  may decrease to less than 10 % along capillaries, which may be shorter than one millimetre in length. To properly account for the mass balance throughout the capillary-tissue exchange region, it is necessary to compute the changes associated with the nonlinear biochemical O<sub>2</sub>–CO<sub>2</sub> interactions in blood as influenced by  $P_{\text{O}_2}$ ,  $P_{\text{CO}_2}$ , pH, and  $T$ , thus the need for accurate and efficient forward and invertible  $S_{\text{HbO}_2}$  and  $S_{\text{HbCO}_2}$  equations.

In order to quantify the Bohr and Haldane effects as well as the synergistic effects of 2,3-DPG and  $T$ , Dash and Bassingthwaighte (2004, 2010) have developed new mathematical models of O<sub>2</sub> and CO<sub>2</sub> saturation of Hb ( $S_{\text{HbO}_2}$  and  $S_{\text{HbCO}_2}$ ) based on equilibrium binding of O<sub>2</sub> and CO<sub>2</sub> to Hb inside RBCs. They are in the form of an invertible Hill-type equation with apparent binding constants  $K_{\text{HbO}_2}$  and  $K_{\text{HbCO}_2}$  which depend on the levels of  $P_{\text{O}_2}$ ,  $P_{\text{CO}_2}$ , pH, 2,3-DPG, and  $T$  in blood. The invertibility of these new equations enables analytical calculations of  $P_{\text{O}_2}$  from  $S_{\text{HbO}_2}$  and  $P_{\text{CO}_2}$  from  $S_{\text{HbCO}_2}$  and vice versa. This is especially important for the integrated computational modeling of simultaneous transport and exchange of O<sub>2</sub> and CO<sub>2</sub> in alveolar-blood and blood-tissue exchange systems (Dash and Bassingthwaighte 2006). The HbO<sub>2</sub> dissociation curves computed from the  $S_{\text{HbO}_2}$  model are in very good agreement with previously published experimental and theoretical curves in the literature over a wide range of physiological conditions (Kelman 1966b; Severinghaus 1979; Winslow et al. 1983; Siggaard-Andersen et al. 1984; Buerk and Bridges 1986). However, as with any theoretical model, there are some limitations in the 2010 Dash and Bassingthwaighte  $S_{\text{HbO}_2}$  and  $S_{\text{HbCO}_2}$  models. In particular, the  $S_{\text{HbO}_2}$  model is only accurate for values of  $S_{\text{HbO}_2}$  lying between 0.3 and 0.98 (with a Hill coefficient  $nH$  of 2.7), even if accounting well in that range for the effects of pH,  $P_{\text{CO}_2}$ , 2,3-DPG and  $T$ . Furthermore, the  $S_{\text{HbO}_2}$  and  $S_{\text{HbCO}_2}$  models require complicated calculations of the indices  $n_1$ ,  $n_2$ ,  $n_3$ , and  $n_4$  involved in the expression for the apparent equilibrium constant in a single-step O<sub>2</sub>–Hb binding reaction (Dash and Bassingthwaighte 2010). These limitations are addressed here by simplifying the  $S_{\text{HbO}_2}$  and  $S_{\text{HbCO}_2}$  models further and extending the accuracy of the  $S_{\text{HbO}_2}$  model to the whole  $S_{\text{HbO}_2}$  range for the varied physiological conditions. The resulting  $S_{\text{HbO}_2}$  and  $S_{\text{HbCO}_2}$  models are also tested using diverse experimental data available in the literature on the HbO<sub>2</sub> and HbCO<sub>2</sub> dissociation curves for a wide range of physiological conditions (Joels and Pugh 1958; Naeraa et al. 1963; Bauer and Schroder 1972; Hlastala et al. 1977; Matthew et al. 1977; Reeves 1980). This study does not include the buffering of CO<sub>2</sub> in blood as that is covered in our previous work on blood-tissue gas exchange (Dash and Bassingthwaighte 2006) and by Wolf (2013) for whole-body acid–base

and electrolyte balance. Interested readers are referred to our previous article (Dash and Bassingthwaighte 2010) for a historical perspective and details of the mathematical models of  $S_{\text{HbO}_2}$  not covered in this paper.

## Methods

### Simple mathematical expressions for $S_{\text{HbO}_2}$ and $S_{\text{HbCO}_2}$

Based on the detailed nonlinear biochemical interactions of  $\text{O}_2$  and  $\text{CO}_2$  with Hb inside RBCs, Dash and Bassingthwaighte (2010) derived the following mechanistic mathematical expressions for the fractional saturation of Hb with  $\text{O}_2$  and  $\text{CO}_2$  ( $S_{\text{HbO}_2}$  and  $S_{\text{HbCO}_2}$ , respectively):

$$S_{\text{HbO}_2} = \frac{K_{\text{HbO}_2}[\text{O}_2]}{1 + K_{\text{HbO}_2}[\text{O}_2]};$$

$$S_{\text{HbCO}_2} = \frac{K_{\text{HbCO}_2}[\text{CO}_2]}{1 + K_{\text{HbCO}_2}[\text{CO}_2]} \quad (1a,b)$$

Here the concentrations are in moles per liter or M with respect to the water space of RBCs. The concentration of free  $\text{O}_2$  or free  $\text{CO}_2$  in the water space of RBCs may also be expressed in terms of the partial pressure of  $\text{O}_2$  or  $\text{CO}_2$  so that  $[\text{O}_2] = \alpha_{\text{O}_2}P_{\text{O}_2}$  and  $[\text{CO}_2] = \alpha_{\text{CO}_2}P_{\text{CO}_2}$ , where  $\alpha_{\text{O}_2}$  and  $\alpha_{\text{CO}_2}$  are the solubilities of  $\text{O}_2$  and  $\text{CO}_2$  in water, computed from their measured values in plasma (Austin et al. 1963; Hedley-Whyte and Laver 1964) and corrected for the effects of temperature (Kelman 1966a, 1967; Dash and Bassingthwaighte 2010):

$$\alpha_{\text{O}_2} = [1.37 - 1.37 \times 10^{-2}(T - 37) + 5.8 \times 10^{-4}(T - 37)^2] \times [10^{-6} / W_{\text{pl}}] \text{ M/mmHg} \quad (2a)$$

$$\alpha_{\text{CO}_2} = [3.07 - 5.7 \times 10^{-2}(T - 37) + 2 \times 10^{-3}(T - 37)^2] \times [10^{-5} / W_{\text{pl}}] \text{ M/mmHg} \quad (2b)$$

where  $W_{\text{pl}} = 0.94$  is the fractional water space of plasma and  $T$  is in degrees centigrade ( $^{\circ}\text{C}$ ). Thus  $\alpha_{\text{O}_2} = 1.46 \times 10^{-6}$  and  $\alpha_{\text{CO}_2} = 3.27 \times 10^{-5}$  M/mmHg at  $37^{\circ}\text{C}$  (see Table 1). The expressions for  $[\text{O}_2]$  and  $[\text{CO}_2]$  in terms of  $P_{\text{O}_2}$  and  $P_{\text{CO}_2}$  and vice versa are freely interchanged throughout this paper. The apparent equilibrium constants of Hb with  $\text{O}_2$  and  $\text{CO}_2$  ( $K_{\text{HbO}_2}$  and  $K_{\text{HbCO}_2}$  with units of  $\text{M}^{-1}$ ), based on single-step bindings of  $\text{O}_2$  and  $\text{CO}_2$  to Hb, are reproduced here from Dash and Bassingthwaighte (2010) in a simplified form, introducing the new variables  $\Phi_1 - \Phi_4$ :

$$K_{\text{HbO}_2} = \frac{K'_4(K'_3[\text{CO}_2]\Phi_2 + \Phi_4)}{K'_2[\text{CO}_2]\Phi_1 + \Phi_3};$$

$$K_{\text{HbCO}_2} = \frac{K'_2\Phi_1 + K'_3K'_4[\text{O}_2]\Phi_2}{\Phi_3 + K'_4[\text{O}_2]\Phi_4} \quad (3a,b)$$

where the molar concentrations of the gases  $\text{O}_2$  and  $\text{CO}_2$  are used; the terms  $\Phi_1 - \Phi_4$  involving the interactions of  $\text{H}^+$  with Hb-bound  $\text{O}_2$  and  $\text{CO}_2$  are given by:

$$\Phi_1 = 1 + \frac{K''_2}{[\text{H}^+]}; \quad \Phi_2 = 1 + \frac{K''_3}{[\text{H}^+]};$$

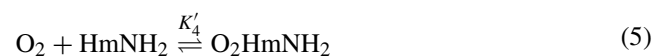
$$\Phi_3 = 1 + \frac{[\text{H}^+]}{K''_5}; \quad \Phi_4 = 1 + \frac{[\text{H}^+]}{K''_6} \quad (4a-d)$$

where  $[\text{H}^+] = 10^{-\text{pH}}$  in RBCs. Given the pH of plasma, the pH of RBCs can be obtained using the simple relationship established by Siggaard-Andersen and colleagues (Siggaard-Andersen 1971; Siggaard-Andersen and Salling 1971):  $\text{pH}_{\text{rbc}} = 0.795\text{pH}_{\text{pl}} + 1.357$ , giving the Gibbs-Donnan ratio for electrochemical equilibrium of  $\text{H}^+$  and  $\text{HCO}_3^-$  across the RBC membrane as a function of  $\text{pH}_{\text{pl}}$ :  $R_{\text{rbc}} = 10^{-(\text{pH}_{\text{pl}} - \text{pH}_{\text{rbc}})} = 10^{-(0.205\text{pH}_{\text{pl}} - 1.357)}$  (see Table 1). In our previous  $S_{\text{HbO}_2}$  and  $S_{\text{HbCO}_2}$  models (Dash and Bassingthwaighte 2010),  $R_{\text{rbc}}$  was considered as a constant:  $R_{\text{rbc}} = 0.69$ , a value corresponding to  $\text{pH}_{\text{pl}} = 7.4$  and  $\text{pH}_{\text{rbc}} = 7.24$  (see Table 1).

With these relationships (Eqs. 1a,b-4a-d), the total  $\text{O}_2$  and  $\text{CO}_2$  concentrations in whole blood can be calculated, as described in the Appendix of the Dash and Bassingthwaighte (2010) paper (see Table 1), and hence are not covered here in detail.

### Dependency of $K'_4$ on the Physiological Variables of Interest

Except for  $K'_4$ , the binding association/dissociation constants are all specified in Table 1.  $K'_4$  represents the single-step binding association constant of  $\text{O}_2$  with each heme chain of Hb ( $\text{HmNH}_2$ ) according to the following hypothetical reaction scheme (Dash and Bassingthwaighte 2010):



The fundamental S-shape of the  $\text{HbO}_2$  dissociation curve results from the form of Eq. 1a and the values taken by the product  $K_{\text{HbO}_2}[\text{O}_2]$ , which depends on  $K'_4$ . For any given range of  $[\text{O}_2]$ , the shifts in the  $\text{HbO}_2$  dissociation curve with respect to varying physiological conditions arise from the dependence of  $K_{\text{HbO}_2}$  on  $[\text{CO}_2]$ ,  $[\text{H}^+]$  (via  $\Phi_1 - \Phi_4$ ), and  $K'_4$ . Similarly, the shape of the  $\text{HbCO}_2$  dissociation curve results from the form of Eq. 1b and the values

**Table 1** Model parameter values used in the simulations, most of which are as presented in the Dash and Bassingthwaite (2010) paper; model parameters that are re-estimated based on fittings of the model to the experimental data in Figs. 1 and 3 are shown with footnotes

| Parameter                            | Definition   | Value   | Unit             |
|--------------------------------------|--|---|------------------|
| $K_1''$                              | Ionization constant of $\text{H}_2\text{CO}_3$   | $5.5 \times 10^{-4}$  | M                |
| $K_1'$                               | Equilibrium constant for the $\text{CO}_2$ hydration reaction: $\text{CO}_2 + \text{H}_2\text{O} \leftrightarrow \text{H}_2\text{CO}_3$ ( $K_1' = K_1 / K_1''$ )   | $1.4 \times 10^{-3}$  | Unitless         |
| $K_1$                                | Equilibrium constant for the overall $\text{CO}_2$ hydration reaction: $\text{CO}_2 + \text{H}_2\text{O} \leftrightarrow \text{HCO}_3^- + \text{H}^+$<br>( $K_1 = K_1' \cdot K_1''$ ); $\text{p}K_1 = -\log_{10}(K_1) = 6.1 - 0.0434(\text{pH}_{\text{pl}} - 7.4) + 0.0014(T - 37)(\text{pH}_{\text{pl}} - 7.4)$<br>( $\text{pH}_{\text{pl}} = 7.4$ ;<br>$T = 37^\circ\text{C}$ )    | $7.94 \times 10^{-7}$   | M                |
| $K_2''$                              | Ionization constant of $\text{HbNHCOOH}$   | $1 \times 10^{-6}$  | M                |
| $K_2'$                               | Equilibrium constant for the $\text{CO}_2$ -Hb binding reaction: $\text{CO}_2 + \text{HbNH}_2 \leftrightarrow \text{HbNHCOOH}$<br>( $K_2' = K_2 / K_2''$ )   | 21.5 <sup>a</sup><br>23.65 <sup>b</sup>                         | $\text{M}^{-1}$  |
| $K_2$                                | Equilibrium constant for the overall $\text{CO}_2$ -Hb binding reaction:<br>$\text{CO}_2 + \text{HbNH}_2 \leftrightarrow \text{HbNHCOO}^- + \text{H}^+$ ( $K_2 = K_2' \cdot K_2''$ )   | $21.5 \times 10^{-6\text{a}}$<br>$23.65 \times 10^{-6\text{b}}$ | Unitless         |
| $K_3''$                              | Ionization constant of $\text{HbO}_2\text{NHCOOH}$   | $1 \times 10^{-6}$  | M                |
| $K_3'$                               | Equilibrium constant for the $\text{CO}_2$ -HbO <sub>2</sub> binding reaction:<br>$\text{CO}_2 + \text{HbO}_2\text{NH}_2 \leftrightarrow \text{HbO}_2\text{NHCOOH}$ ( $K_3' = K_3 / K_3''$ )   | 11.3 <sup>a</sup><br>14.7 <sup>b</sup>                          | $\text{M}^{-1}$  |
| $K_3$                                | Equilibrium constant for the overall $\text{CO}_2$ -HbO <sub>2</sub> binding reaction: $\text{CO}_2 + \text{HbO}_2\text{NH}_2 \leftrightarrow \text{HbO}_2\text{NHCOO}^- + \text{H}^+$ ( $K_3 = K_3' \cdot K_3''$ )  | $11.3 \times 10^{-6\text{a}}$<br>$14.7 \times 10^{-6\text{b}}$  | Unitless         |
| $K_{4,\text{S}}'$                    | Equilibrium constant for the overall $\text{O}_2$ -Hb binding reaction: $\text{O}_2 + \text{HbNH}_2 \leftrightarrow \text{HbO}_2\text{NH}_2$ at standard physiological conditions (otherwise it is a function of $P_{\text{O}_2}$ , $P_{\text{CO}_2}$ , $\text{pH}_{\text{rbc}}$ , $[\text{DPG}]_{\text{rbc}}$ and $T$ )   | $2.03 \times 10^5$  | $\text{M}^{-1}$  |
| $K_5''$                              | Ionization constant of $\text{HbNH}_3^+$   | $2.4 \times 10^{-8\text{a}}$<br>$2.64 \times 10^{-8\text{b}}$   | M                |
| $K_6''$                              | Ionization constant of $\text{HbO}_2\text{NH}_3^+$   | $1.2 \times 10^{-8\text{a}}$<br>$1.56 \times 10^{-8\text{b}}$   | M                |
| $nH$                                 | Hill coefficient with variable cooperativity hypothesis for $\text{O}_2$ binding to Hb:<br>$nH = \alpha - \beta \times 10^{-P_{\text{O}_2}/\gamma}$ (Eq. 11)   | Variable  | Unitless         |
| $\alpha$                             | Parameter governing $P_{\text{O}_2}$ -dependent variable Hill coefficient $nH$ with variable cooperativity hypothesis for $\text{O}_2$ binding to Hb   | 2.82 <sup>c</sup>   | Unitless         |
| $\beta$                              | Parameter governing $P_{\text{O}_2}$ -dependent variable Hill coefficient $nH$ with variable cooperativity hypothesis for $\text{O}_2$ binding to Hb   | 1.20 <sup>c</sup>   | Unitless         |
| $\gamma$                             | Parameter governing $P_{\text{O}_2}$ -dependent variable Hill coefficient $nH$ with variable cooperativity hypothesis for $\text{O}_2$ binding to Hb   | 29.25 <sup>c</sup>  | mmHg             |
| $P_{50,\text{S}}$                    | Level of $P_{\text{O}_2}$ at which Hb is 50 % saturated by $\text{O}_2$ at standard physiological levels of $P_{\text{CO}_2}$ , $\text{pH}_{\text{rbc}}$ , $[\text{DPG}]_{\text{rbc}}$ and $T$   | 26.8 <sup>c</sup>   | mmHg             |
| $P_{\text{O}_2,\text{S}}$            | Standard partial pressure of $\text{O}_2$ in blood   | 100   | mmHg             |
| $P_{\text{CO}_2,\text{S}}$           | Standard partial pressure of $\text{CO}_2$ in blood  | 40  | mmHg             |
| $\text{pH}_{\text{pl},\text{S}}$     | Standard pH in plasma  | 7.4   | Unitless         |
| $\text{pH}_{\text{rbc},\text{S}}$    | Standard pH in RBCs, related to the standard plasma pH by: $\text{pH}_{\text{rbc},\text{S}} = 0.795\text{pH}_{\text{pl},\text{S}} + 1.357$   | 7.24  | Unitless         |
| $[\text{DPG}]_{\text{rbc},\text{S}}$ | Standard 2,3-DPG concentration in RBCs   | $4.65 \times 10^{-3}$   | M                |
| $T_{\text{S}}$                       | Standard temperature of blood  | 37  | $^\circ\text{C}$ |
| $\text{pH}_{\text{rbc}}$             | pH in RBCs, related to plasma pH by: $\text{pH}_{\text{rbc}} = 0.795\text{pH}_{\text{pl}} + 1.357$   | Variable  | Unitless         |
| $R_{\text{rbc}}$                     | Gibbs-Donnan ratio for electrochemical equilibrium of protons or bicarbonate ions across the RBC membrane ( $R_{\text{rbc}} = [\text{H}^+]_{\text{pl}} / [\text{H}^+]_{\text{rbc}} = [\text{HCO}_3^-]_{\text{rbc}} / [\text{HCO}_3^-]_{\text{pl}}$ ; $R_{\text{rbc}} = 10^{-(\text{pH}_{\text{pl}} - \text{pH}_{\text{rbc}})} = 10^{-(0.205 \cdot \text{pH}_{\text{pl}} - 1.357)}$ ) | Variable (0.692 at $\text{pH}_{\text{pl}} = 7.4$ )              | Unitless         |
| $\alpha_{\text{O}_2,\text{S}}$       | Solubility of $\text{O}_2$ in water at standard temperature ( $37^\circ\text{C}$ )   | $1.46 \times 10^{-6}$   | M/mmHg           |
| $\alpha_{\text{CO}_2,\text{S}}$      | Solubility of $\text{CO}_2$ in water at standard temperature ( $37^\circ\text{C}$ )  | $3.27 \times 10^{-5}$   | M/mmHg           |
| $\text{Hct}_{\text{S}}$              | Standard hematocrit (volume fraction of RBCs in blood)   | 0.45  | Unitless         |
| $[\text{Hb}]_{\text{bl},\text{S}}$   | Standard hemoglobin concentration in blood   | $2.33 \times 10^{-3}$   | M                |
| $[\text{Hb}]_{\text{rbc},\text{S}}$  | Standard hemoglobin concentration in RBCs ( $[\text{Hb}]_{\text{rbc}} = [\text{Hb}]_{\text{bl}} / \text{Hct}$ )  | $5.18 \times 10^{-3}$   | M                |
| $W_{\text{pl}}$                      | Fractional water space of plasma   | 0.94  | Unitless         |
| $W_{\text{rbc}}$                     | Fractional water space of RBCs   | 0.65  | Unitless         |
| $W_{\text{bl}}$                      | Fractional water space of blood: $W_{\text{bl}} = (1 - \text{Hct}) \cdot W_{\text{pl}} + \text{Hct} \cdot W_{\text{rbc}}$  | 0.81  | Unitless         |
| $[\text{O}_2]_{\text{tot}}$          | Total $\text{O}_2$ concentration of whole blood: $[\text{O}_2]_{\text{tot}} = W_{\text{bl}} \cdot \alpha_{\text{O}_2} \cdot P_{\text{O}_2} + 4 \cdot \text{Hct} \cdot [\text{Hb}]_{\text{rbc}} \cdot S_{\text{HbO}_2}$   | Variable  | M                |

**Table 1** continued

| Parameter      | Definition   | Value    | Unit |
|----------------|--|----------|------|
| $[CO_2]_{tot}$ | Total $CO_2$ concentration of whole blood: $[CO_2]_{tot} = W_{bl} \cdot \alpha_{CO_2} \cdot P_{CO_2} + ((1-Hct)W_{pl} + Hct \cdot W_{rbc} \cdot R_{rbc})(K_1 \cdot \alpha_{CO_2} \cdot P_{CO_2} / [H^+]_{pl}) + 4 \cdot Hct \cdot [Hb]_{rbc} \cdot S_{HbCO_2}$ (parameter $K_1$ defined above) | Variable | M    |

<sup>a</sup> Estimated based on model fittings to the data of Bauer and Schröder (1972) at  $T = 37^\circ C$  (see Fig. 3e)

<sup>b</sup> Estimated based on model fittings to the data of Matthew et al. (1977) at  $T = 30^\circ C$  (see Fig. 3f)

<sup>c</sup> Estimated based on model fittings to the data of Severinghaus and colleagues (Roughton and Severinghaus 1973; Roughton and Severinghaus 1973; Severinghaus 1979) in normal human blood at standard physiological conditions

Unless otherwise noted, the kinetic parameter values are at  $T = 37^\circ C$

taken by the product  $K_{HbCO_2} [CO_2]$ , which also depends on  $K'_4$ . For any given range of  $[CO_2]$ , the shifts in the  $HbCO_2$  dissociation curve with respect to varying physiological conditions arise from the dependence of  $K_{HbCO_2}$  on  $[O_2]$ ,  $[H^+]$  (via  $\Phi_1 - \Phi_4$ ), and  $K'_4$ . From the above description, it is clear that determining  $K'_4$  is a critical step in the application of Eq. 1a,b. In our previous  $S_{HbO_2}$  and  $S_{HbCO_2}$  models (Dash and Bassingthwaite 2010),  $K'_4$  is expressed as a complicated function of  $[O_2]$ ,  $[CO_2]$ ,  $[H^+]$ , [DPG] and  $T$  involving the exponents  $n_0, n_1, n_2, n_3$  and  $n_4$ , which, except for  $n_0$  (a constant equal to 1.7), are themselves complicated functions of these physiological variables and  $P_{50}$  of  $O_2$ . In the section below, we show how a very simple expression for  $K'_4$  can be obtained without involving the exponents  $n_0-n_4$ , significantly simplifying the  $S_{HbO_2}$  and  $S_{HbCO_2}$  models.

**Derivation of simple mathematical expression for  $K'_4$**

Hill’s exponent model for  $S_{HbO_2}$  is based on an  $n$ th-order one-step binding of Hb with  $O_2$ :

$$S_{HbO_2} = \frac{(P_{O_2}/P_{50})^n}{1 + (P_{O_2}/P_{50})^n} \tag{6}$$

Here  $n = nH$ , the Hill coefficient, is approximately 2.7 for normal human blood;  $P_{50}$  is the value of  $P_{O_2}$  at which Hb is 50 % saturated by  $O_2$ . In Eq. 6, the shifts of the  $HbO_2$  dissociation curve produced by varying physiological conditions arise because  $P_{50}$  is a function of  $P_{CO_2}$ , pH, [DPG] and  $T$ , as described below. If Eqs. 1a and 6 are to give identical  $HbO_2$  dissociation curves, we must have  $K_{HbO_2} \alpha_{O_2} P_{O_2} = (P_{O_2}/P_{50})^{nH}$ , which when simplified gives:

$$K'_4 = \frac{(\alpha_{O_2} P_{O_2})^{nH-1} (K'_2 \alpha_{CO_2} P_{CO_2} \Phi_1 + \Phi_3)}{(\alpha_{O_2} P_{50})^{nH} (K'_3 \alpha_{CO_2} P_{CO_2} \Phi_2 + \Phi_4)} \tag{7}$$

While it is simple to compute  $S_{HbO_2}$  from Eq. 6, this is not true for  $S_{HbCO_2}$ . However, Eq. 7 provides an expression for  $K'_4$  in terms of  $P_{O_2}$ ,  $P_{CO_2}$ , pH and  $P_{50}$ , which along with Eqs. 1b and 3b describes a simplified model for the  $HbCO_2$  dissociation curve. Note also that Eq. 7 can be written in the following alternative form:

$$K'_4 = \left( \frac{1}{\alpha_{O_2} P_{O_2}} \right) \left( \frac{S_{HbO_2}}{1 - S_{HbO_2}} \right) \left( \frac{K'_2 \alpha_{CO_2} P_{CO_2} \Phi_1 + \Phi_3}{K'_3 \alpha_{CO_2} P_{CO_2} \Phi_2 + \Phi_4} \right) \tag{8}$$

so that as  $S_{HbO_2}$  approaches 1,  $K'_4$  becomes infinitely large and  $K_{HbCO_2}$  becomes equal to  $K'_3 \Phi_2 / \Phi_4$  in Eq. 3b. If a “Division by Zero” error is to be avoided when calculating  $K_{HbCO_2}$  in computer programs based on these equations, it is necessary to identify situations in which  $S_{HbO_2}$  might equal 1 (at very high  $P_{O_2}$ ), bypass Eq. 7, and immediately set  $K_{HbCO_2}$  to  $K'_3 \Phi_2 / \Phi_4$ .

**Simple mathematical expression for  $P_{50}$  of  $O_2$**

$P_{50}$  is a function of  $P_{CO_2}$ , pH, [DPG] and  $T$ . Dash and Bassingthwaite (2010) obtained a polynomial expression for  $P_{50}$  by varying one of these variables at a time, while keeping the other three fixed at their standard physiological values. The resulting polynomial expressions for  $P_{50,\Delta pH}$ ,  $P_{50,\Delta CO_2}$ ,  $P_{50,\Delta DPG}$ , and  $P_{50,\Delta T}$  were fitted to the reported  $P_{50}$  data from the studies of Buerk and Bridges (1986) and Winslow et al. (1983). These polynomial expressions from Dash and Bassingthwaite (2010) are further refined here based on additional experimental data from Joels and Pugh (1958), Naeraa et al. (1963), Hlastala et al. (1977), and Reeves (Reeves 1980) that provide appropriate shifts in  $S_{HbO_2}$  with varying pH,  $P_{CO_2}$  and  $T$ :

$$P_{50,\Delta pH} = P_{50,S} - 25.535 (pH - pH_S) + 10.646 (pH - pH_S)^2 - 1.764 (pH - pH_S)^3 \tag{9a}$$

$$P_{50,\Delta CO_2} = P_{50,S} + 1.273 \times 10^{-1} (P_{CO_2} - P_{CO_2,S}) + 1.083 \times 10^{-4} (P_{CO_2} - P_{CO_2,S})^2 \tag{9b}$$

$$P_{50,\Delta DPG} = P_{50,S} + 795.63 ([DPG] - [DPG]_S) - 19660.89 ([DPG] - [DPG]_S)^2 \tag{9c}$$

$$P_{50,\Delta T} = P_{50,S} + 1.435 (T - T_S) + 4.163 \times 10^{-2} (T - T_S)^2 + 6.86 \times 10^{-4} (T - T_S)^3 \tag{9d}$$

where the standard physiological values are denoted by the subscript “S” and are listed in Table 1. The accuracy of the expression for  $P_{50,\Delta\text{pH}}$  at extreme pH levels has been further improved in Eq. 9a by incorporating the cubic term. Previous researchers (Kelman 1966b; Severinghaus 1979; Siggaard-Andersen et al. 1984; Buerk and Bridges 1986) have shown that for the calculation of  $P_{50}$  to be valid when multiple physiological variables are allowed to vary simultaneously, the contribution of each physiological variable to the resulting  $P_{50}$  is by multiplication of normalized individual  $P_{50}$ 's. Consequently, the expression for  $P_{50}$  that best describes the simultaneous varying physiological conditions is given by:

$$P_{50} = P_{50,S} \left( \frac{P_{50,\Delta\text{pH}}}{P_{50,S}} \right) \left( \frac{P_{50,\Delta\text{CO}_2}}{P_{50,S}} \right) \times \left( \frac{P_{50,\Delta\text{DPG}}}{P_{50,S}} \right) \left( \frac{P_{50,\Delta\text{T}}}{P_{50,S}} \right) \quad (10)$$

### Incorporation of the variable cooperativity hypothesis

In our previous  $S_{\text{HbO}_2}$  and  $S_{\text{HbCO}_2}$  models (Dash and Basingthwaite 2010), the Hill coefficient  $nH$  was fixed at 2.7 (or  $n_0$  was fixed at 1.7), making the  $S_{\text{HbO}_2}$  accurate only between 30 and 98 %. Next, we extend the accuracy of the modified  $S_{\text{HbO}_2}$  model for the whole saturation range by incorporating an empirical  $P_{\text{O}_2}$ -dependent variable cooperativity hypothesis for  $\text{O}_2$  binding to Hb. Specifically, this is achieved by expressing the Hill coefficient  $nH$  at low  $P_{\text{O}_2}$  as a simple exponential function of  $P_{\text{O}_2}$ :

$$nH = \alpha - \beta \times 10^{-(P_{\text{O}_2}/\gamma)} \quad (11)$$

where  $\alpha$ ,  $\beta$  and  $\gamma$  are parameters that govern an apparent cooperativity of  $\text{O}_2$  for Hb. Equation 11 suggests that at low  $P_{\text{O}_2}$ ,  $nH$  is close to  $\alpha - \beta$ , but increases exponentially towards  $\alpha$  with the rate  $\gamma$  as  $P_{\text{O}_2}$  increases. These three parameters along with  $P_{50,S}$  are estimated here based on fittings of the  $S_{\text{HbO}_2}$  model to the available experimental data of Severinghaus and colleagues (Roughton et al. 1972; Roughton and Severinghaus 1973; Severinghaus 1979) and Winslow et al. (1977) on normal human blood  $\text{HbO}_2$  dissociation curves at standard physiological conditions. With  $nH$  accurately defined by Eq. 11, suitable shifts in the  $\text{HbO}_2$  and  $\text{HbCO}_2$  dissociation curves are achieved through our new expressions for  $P_{50}$  (Eqs. 9 and 10) and  $K'_4$  (Eq. 7).

### Efficient numerical inversion of the $S_{\text{HbO}_2}$ and $S_{\text{HbCO}_2}$ expressions for practical usage

Equation 1a for  $\text{HbO}_2$  saturation ( $S_{\text{HbO}_2}$ ) is not convenient for analytical inversion, because the apparent equilibrium constant  $K_{\text{HbO}_2}$  for the binding of  $\text{O}_2$  to Hb depends on  $K'_4$ , which in turn depends on  $P_{\text{O}_2}$  (see Eq. 7). However, since Eq. 1a is equivalent to Eq. 6, which depends on  $P_{50}$ , which

in turn is independent of  $P_{\text{O}_2}$  and is only a function of pH,  $P_{\text{CO}_2}$ , [DPG] and  $T$ , Eq. 6 can be analytically inverted to compute  $P_{\text{O}_2}$  from  $S_{\text{HbO}_2}$ , subject to the condition that the Hill coefficient  $nH$  is a constant. When  $nH$  is allowed to vary with  $P_{\text{O}_2}$ , Eq. 6 can no longer be inverted analytically. However, numerical inversion is possible using efficient iterative schemes such as those presented in the Appendix to this paper. These converge within 8 or less iterations when appropriate starting values are used for  $P_{\text{O}_2}$ . The same approach holds for the inversion of Eq. 1b in the computation of  $P_{\text{CO}_2}$  from  $S_{\text{HbCO}_2}$  (see “Appendix”), which may not be important clinically, but is of relevance in the integrated computational modeling of simultaneous transport and exchange of respiratory gases in physiological systems. Two efficient numerical methods are presented in the Appendix for the inversion of each gas, based on fixed-point and quasi-Newton–Raphson iteration methods. Similar iterative methods can be used to compute  $P_{\text{O}_2}$  and  $P_{\text{CO}_2}$  from the total  $[\text{O}_2]$  and the total  $[\text{CO}_2]$ , respectively (these last two parameters are defined in Table 1).

## Results

The effect of varying the Hill coefficient  $nH$  as a function of  $P_{\text{O}_2}$  on the modified  $S_{\text{HbO}_2}$  model simulations at standard physiological conditions is demonstrated through Fig. 1, in which Fig. 1a, c, e are based on the data of Severinghaus and colleagues (Roughton et al. 1972; Roughton and Severinghaus 1973; Severinghaus 1979), while Fig. 1b, d, f are based on the data of Winslow et al. (1977). The first diagram in each set shows how the old and new  $S_{\text{HbO}_2}$  models (constant and variable  $nH$ ) fit the data in the  $P_{\text{O}_2}$  range of 0–150 mmHg. The inset in each of these two figures shows the fit in the lower  $P_{\text{O}_2}$  range of 0–30 mmHg. It is immediately apparent that the previous  $S_{\text{HbO}_2}$  model, which does not incorporate the variable cooperativity hypothesis, produces a poor fit in the lower 40 % saturation range. In Fig. 1c, d, the residual error in the computed  $S_{\text{HbO}_2}$  relative to the experimental  $S_{\text{HbO}_2}$  is shown for each model for the range of values taken by  $S_{\text{HbO}_2}$ . When the saturation is <40 %, the residual error is much improved for the new  $S_{\text{HbO}_2}$  model (<0.05 % for variable  $nH$  compared to ~3–4 % for constant  $nH$ ), and the average residual error over the whole saturation range is virtually zero. Figure 1e, f show how this improvement has been achieved by varying the Hill coefficient  $nH$  in the low  $P_{\text{O}_2}$  range through the application of Eq. 11 (solid line), compared with the constant value used for  $nH$  in the old  $S_{\text{HbO}_2}$  model (dashed line). We note here that the  $nH$  rate parameter  $\gamma$  is related to the  $P_{50,S}$  value, which differs slightly for the two different data sets (26.8 vs. 29.1 mmHg). To achieve the best fit, the parameters  $\alpha$  and  $\beta$  also differ slightly between the

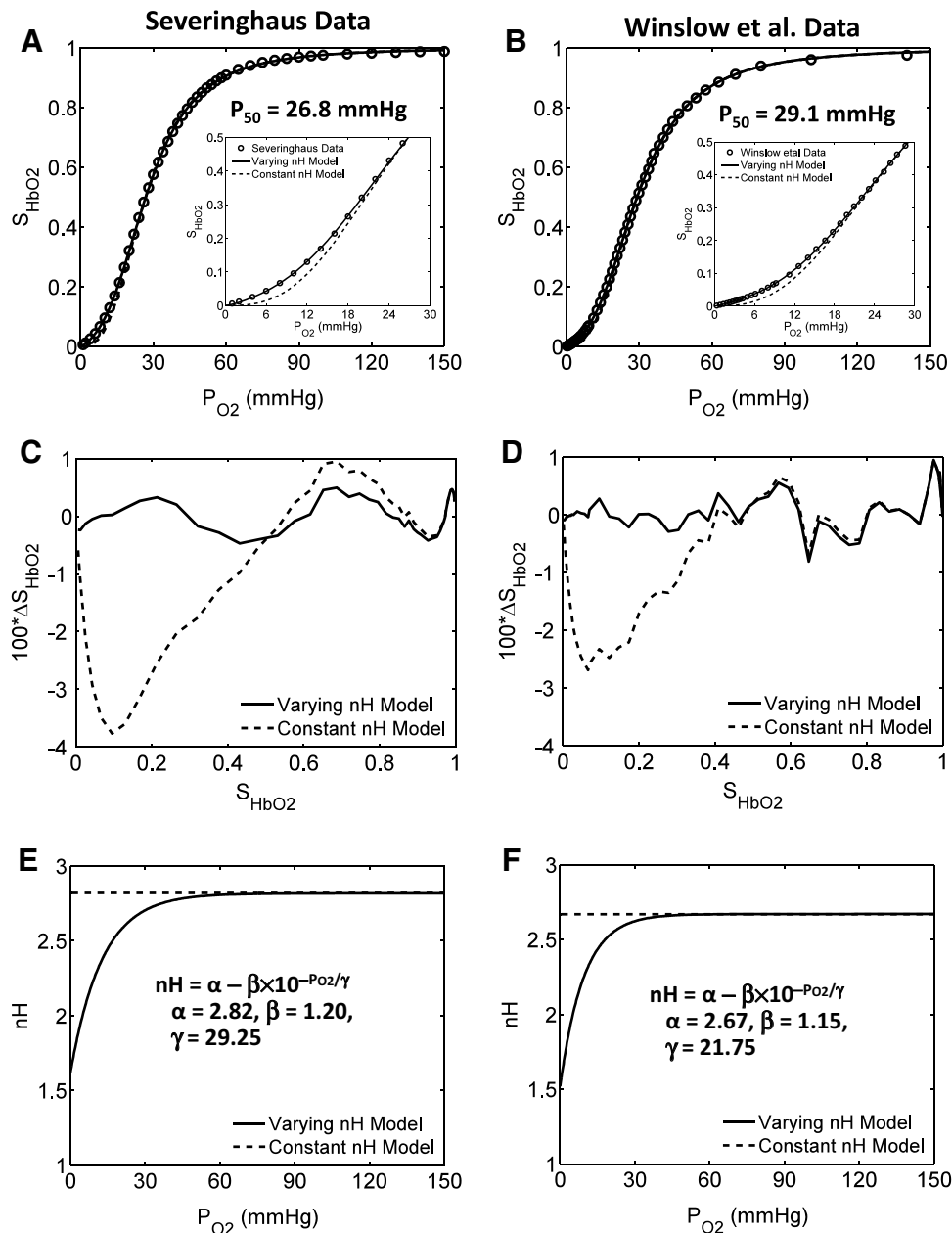


**Fig. 1** Illustration of the accuracy of the modified  $S_{HbO_2}$  model under standard physiological conditions with  $P_{O_2}$ -dependent variable cooperativity hypothesis for  $O_2$ -Hb binding. **a, b** Comparison of the model-simulated  $HbO_2$  dissociation curves with constant and variable cooperativity hypotheses for  $O_2$ -Hb binding (constant and variable Hill coefficient  $nH$ ) to available experimental data in the literature, on normal human blood at standard physiological conditions. The simulations in *panel a* are compared to the data of Severinghaus et al. (Roughton and Severinghaus 1973; Roughton and Severinghaus 1973; Severinghaus 1979), and those in *panel b* are compared to the data of Winslow et al. (1977). The simulations in the main plots are compared to the data over the whole  $S_{HbO_2}$  range, while those in the inset plots are compared to the data for  $S_{HbO_2} \leq 0.5$ , effectively demonstrating the improved accuracy of the modified  $S_{HbO_2}$  model with variable  $nH$  in simulating the data in the lower  $S_{HbO_2}$  range. **c, d** The

percentage deviations ( $100 \times \Delta S_{HbO_2}$ ) of the model-simulated  $S_{HbO_2}$  values from the experimental  $S_{HbO_2}$  values for the constant and variable  $nH$  models plotted as functions of  $S_{HbO_2}$  for the data of Severinghaus and colleagues (Roughton and Severinghaus 1973; Roughton and Severinghaus 1973; Severinghaus 1979); Winslow et al. (1977). The incorporation of the variable cooperativity hypothesis for  $O_2$ -Hb binding (variable  $nH$ ) has improved the accuracy of the  $S_{HbO_2}$  model. **e, f** The  $P_{O_2}$ -dependent variation of  $nH$  corresponding to the constant and variable cooperativity hypotheses for  $O_2$ -Hb binding that are obtained based on fittings of the modified  $S_{HbO_2}$  model to the data of Severinghaus and colleagues (Roughton and Severinghaus 1973; Roughton and Severinghaus 1973; Severinghaus 1979); Winslow et al. (1977). The insets in plots (**e, f**) show the expressions for the variable  $nH$  and the governing parameter values for the two data sets

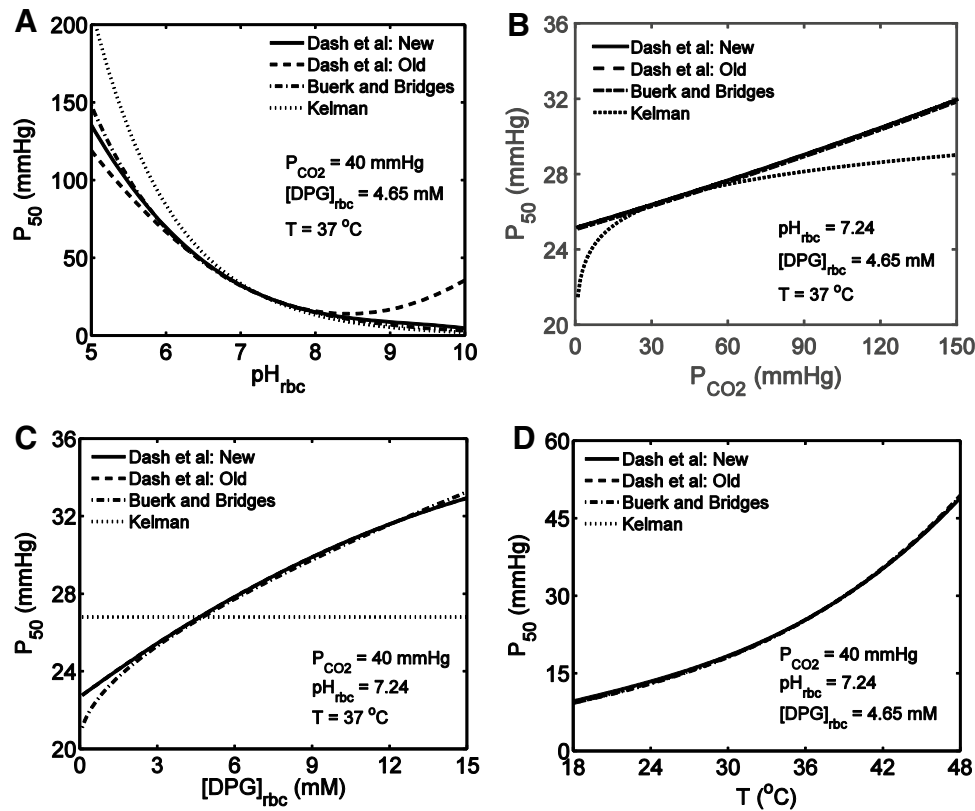


**Fig. 2** Comparison of  $P_{50}$  values under various physiological conditions based on simulations of different  $P_{50}$  models. **a–d** Comparison of the modified  $P_{50}$  model (Eqs. 9, 10) with the previous  $P_{50}$  models from the literature (Kelman 1966b; Buerk and Bridges 1986; Dash and Bassingthwaite 2010), in which the model-simulated  $P_{50}$  values are plotted as functions of one variable with the other variables fixed at their standard physiological values; i.e.  $P_{50}$  as a function of  $\text{pH}_{\text{rbc}}$

(**a**),  $P_{\text{CO}_2}$  (**b**),  $[\text{DPG}]_{\text{rbc}}$  (**c**), and  $T$  (**d**). The  $P_{50}$  values have been computed from Eqs. 9 and 10 under varying physiological conditions with appropriate multiplicative factors (0.833, 0.588 and 1.02 for  $P_{50,\Delta\text{pH}}$ ,  $P_{50,\Delta\text{CO}_2}$  and  $P_{50,\Delta T}$ , respectively) to allow a comparison with the previous models, which have not been adjusted to account for the data of Joels and Pugh (1958), Naeraa et al. (1963), Hlastala et al. (1977) and Reeves (1980)

two different sets of data. This improved accuracy in  $S_{\text{HbO}_2}$  at low  $P_{\text{O}_2}$  may not be relevant clinically, but is important for the computational modeling and mechanistic understanding of in vitro and in vivo blood gas data under non-physiological conditions, such as ischemia and reperfusion, extremes in gas concentrations, high altitudes, and extreme temperatures.

The  $P_{50}$  values computed from Eqs. 9 and 10 under varying physiological conditions are plotted in Fig. 2a–d and are compared to those computed from alternative models from the literature (Kelman 1967; Buerk and Bridges 1986; Dash and Bassingthwaite 2010). The alternative models do not include corrections based on the experimental data of Joels and Pugh (1958), Naeraa et al. (1963), Hlastala et al. (1977) and Reeves (1980); so for the purpose of this comparison, these corrections have been omitted from Eqs. 9a–d by applying appropriate scaling factors of 0.833, 0.588 and 1.02 for  $P_{50,\Delta\text{pH}}$ ,  $P_{50,\Delta\text{CO}_2}$  and  $P_{50,\Delta T}$ , respectively. These simulations show that our scaled  $P_{50}$

values agree well with those computed from the model of Buerk and Bridges (1986), that are based on the studies of Winslow et al. (1983). However, they do differ from the  $P_{50}$  values computed from the model of Kelman (1966b), where it fails to fit the data at low pH and at either very low or very high  $P_{\text{CO}_2}$ . Our scaled  $P_{50}$  values are also improved from our old  $P_{50}$  values for  $\text{pH} > 8.5$  with the incorporation of the cubic term in Eq. 9a. In addition, the inclusion of corrections based on the diverse experimental data sets of Joels and Pugh (1958), Naeraa et al. (1963), Hlastala et al. (1977), and Reeves (1980) in Eqs. 9(a–d) provides further improvement in the  $P_{50}$  values over a wide range of variation in the relevant physiological variables (see description below for Fig. 3). A new model recently published by Matejak et al. (2015), while this article was under preparation, also fits some of these experimental data well under altered physiological conditions. Their approach, a modification of Adair’s four-step algorithm (Adair 1925), considers the problems in depth, and,



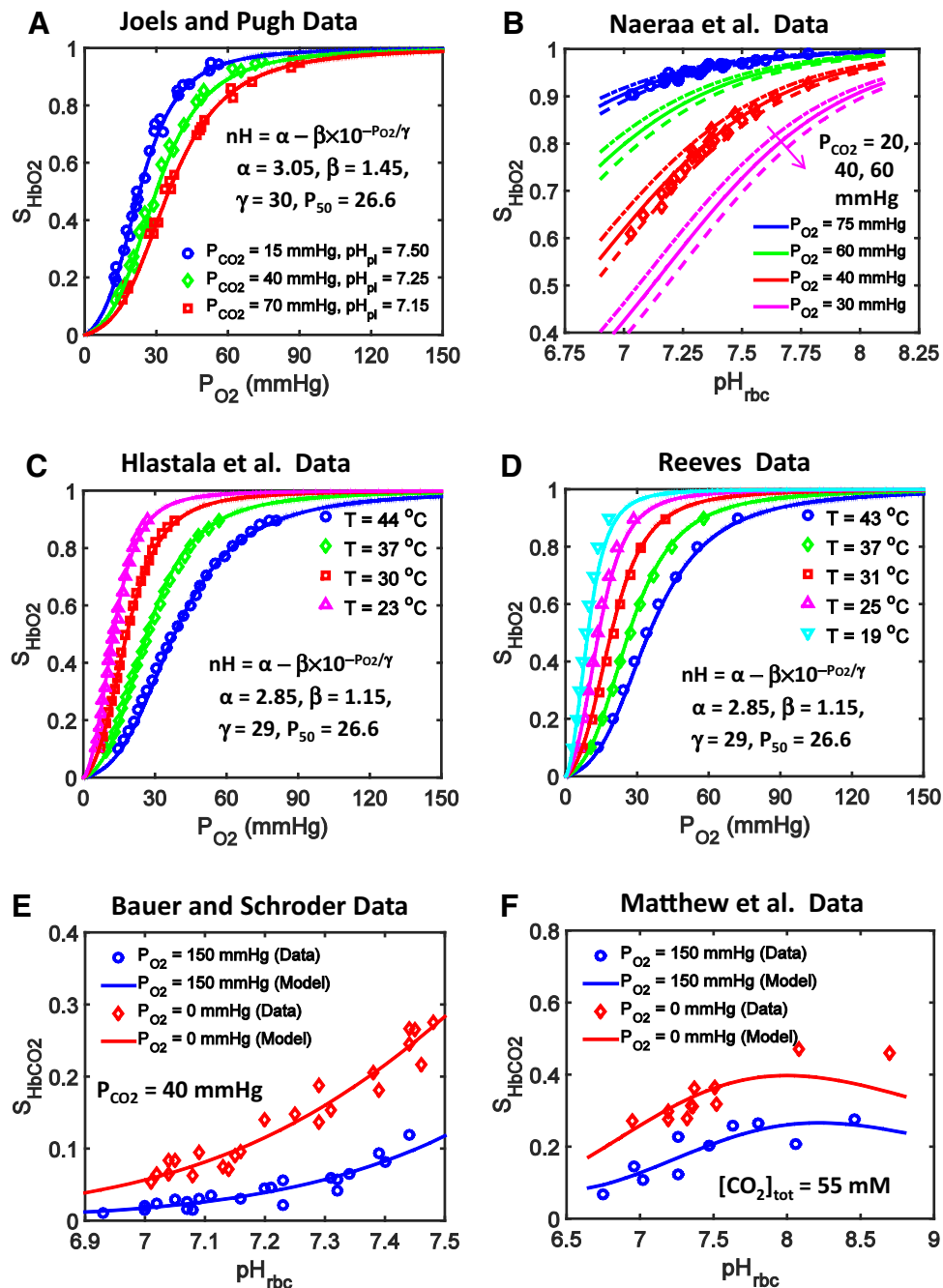
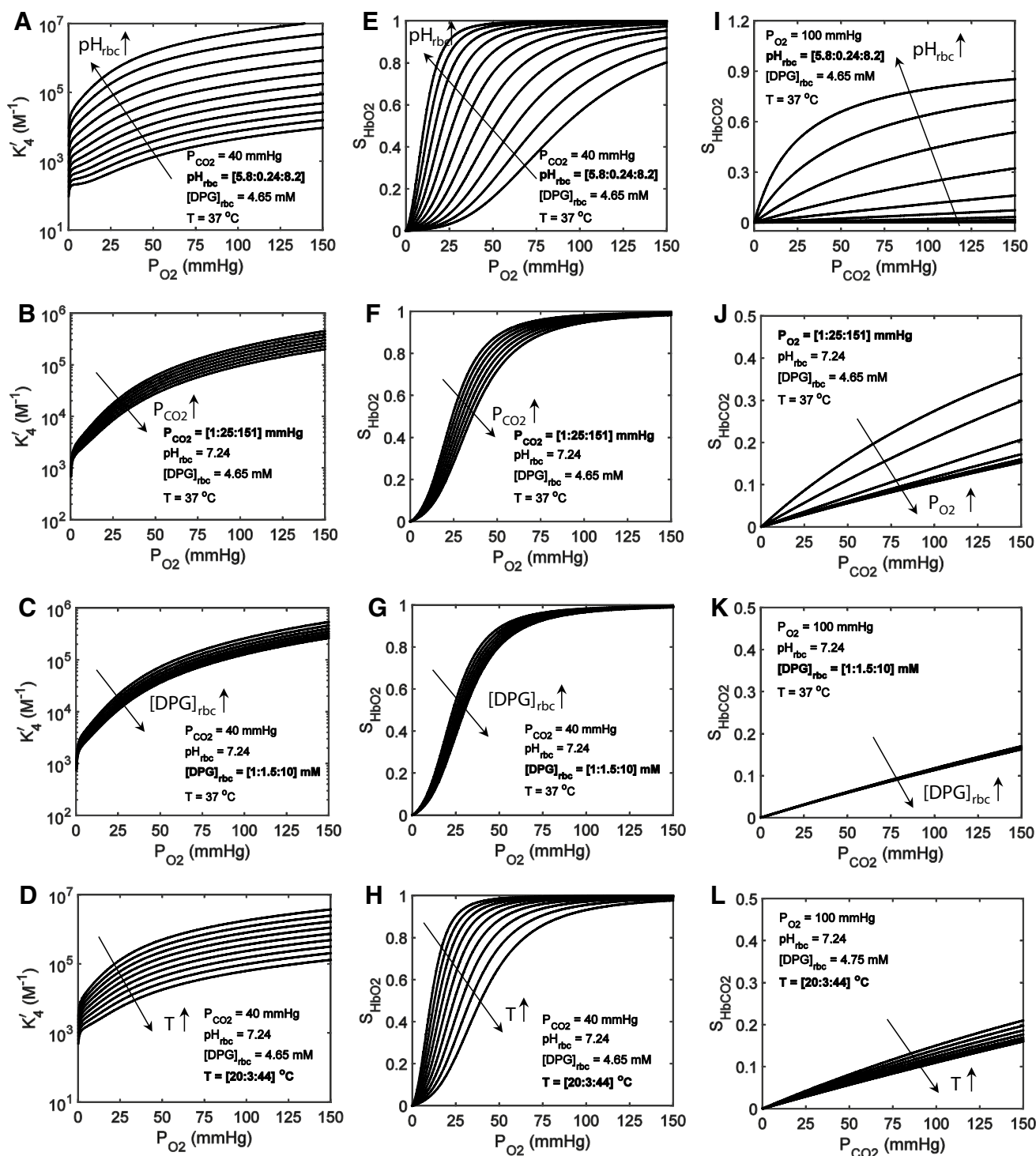


**Fig. 3** Comparison of our improved  $S_{HbO_2}$  and  $S_{HbCO_2}$  model simulations to the diverse experimental data available in the literature under non-standard physiological conditions. **a**  $HbO_2$  dissociation curves obtained from our improved  $S_{HbO_2}$  model (i.e., modified  $S_{HbO_2}$  model with variable cooperativity hypothesis for  $O_2$ –Hb binding (variable  $nH$ )) compared with the data of Joels and Pugh (1958) obtained at various  $pH_{pl}$  and  $P_{CO_2}$  levels with  $T = 37$  °C. The inset shows the expression for the variable  $nH$  and the governing parameter values that produce the best fit of the model to these data sets. In addition, these model fittings characterize the pH and  $P_{CO_2}$  dependencies of  $P_{50}$  in Eqs. 9a and 9b. **b**  $S_{HbO_2}$  levels obtained from our improved  $S_{HbO_2}$  model compared to the data of Naeraa et al. (1963) obtained as a function of  $pH_{rbc}$  for different  $P_{O_2}$  and  $P_{CO_2}$  levels at 37 °C. Other details are as for panel a. **c, d**  $HbO_2$  dissociation curves obtained from our improved  $S_{HbO_2}$

model compared with the data of Hlastala et al. (1977) and Reeves (1980) obtained for various values of  $T$  with  $pH_{pl}$  and  $P_{CO_2}$  fixed at 7.4 and 40 mmHg, respectively. The insets show the expression for the variable  $nH$  and the governing parameter values that enable best fits of the model to these data sets. In addition, these model fittings characterize the temperature dependency of  $P_{50}$  in Eq. 9d. **e, f**  $S_{HbCO_2}$  levels obtained from our improved  $S_{HbCO_2}$  model compared with the data of Bauer and Schröder (1972) and Matthew et al. (1977) obtained as a function of  $pH_{rbc}$  in the oxygenated (high  $P_{O_2}$ ) and deoxygenated (zero  $P_{O_2}$ ) blood with  $P_{CO_2}$  fixed at 40 mmHg ( $T = 37$  °C) in the former experiments and total  $[CO_2]$  fixed at 55 mM ( $T = 30$  °C) in the latter experiments. These model fittings provide the estimates of the equilibrium constants associated with the binding of  $CO_2$  to oxygenated and deoxygenated Hb as well as the ionization constants of oxygenated and deoxygenated Hb



like ours, relates the  $O_2$ -Hb and  $CO_2$ -Hb binding effects to the acid–base chemistry of blood based on pH and  $P_{CO_2}$ , as proposed by Siggaard-Andersen and others over the years (Rossi-Bernardi and Roughton 1967; Forster et al. 1968; Siggaard-Andersen 1971; Siggaard-Andersen and Salling 1971; Bauer and Schroder 1972; Siggaard-Andersen et al. 1972a, b; Siggaard-Andersen and Garby

1973; Siggaard-Andersen et al. 1984; Siggaard-Andersen and Siggaard-Andersen 1990). Specifically, they effectively express the four Adair coefficients in terms of the physiological variables of interest (i.e. pH,  $P_{CO_2}$ , and  $T$ )—they do not consider the effects of 2,3-DPG), providing appropriate shifts in the  $HbO_2$  dissociation curve with altered physiological conditions.

◀ **Fig. 4** Simulations of the apparent HbO<sub>2</sub> binding constant  $K'_4$  (a–d), HbO<sub>2</sub> dissociation curves (e–h), and HbCO<sub>2</sub> dissociation curves (i–l) under varying physiological conditions based on our modified models of  $K'_4$ ,  $S_{\text{HbO}_2}$  and  $S_{\text{HbCO}_2}$  with the  $P_{\text{O}_2}$ -dependent variable cooperativity hypothesis for O<sub>2</sub>-Hb binding. In plots (a–d) and (e–h), the simulations of  $K'_4$  and  $S_{\text{HbO}_2}$  are shown as functions of  $P_{\text{O}_2}$ , respectively, while in plots (i–l), the simulations of  $S_{\text{HbCO}_2}$  are shown as a function of  $P_{\text{CO}_2}$ . The values of the variables used in each simulation are shown as insets in each panel. Three of the variables are fixed at their standard physiological values, while the fourth one is allowed to increase from a low value to a high value by predetermined increments, shown by the sequence [low: increment: high]. Specifically, in plots (a, e, i), pH<sub>rbc</sub> varies, while either  $P_{\text{CO}_2}$  or  $P_{\text{O}_2}$ , [DPG]<sub>rbc</sub> and  $T$  are fixed; in plots (b, f, j), either  $P_{\text{CO}_2}$  or  $P_{\text{O}_2}$  varies, while pH<sub>rbc</sub>, [DPG]<sub>rbc</sub> and  $T$  are fixed; in plots (c, g, k), [DPG]<sub>rbc</sub> varies, while pH<sub>rbc</sub>, either  $P_{\text{CO}_2}$  or  $P_{\text{O}_2}$ , and  $T$  are fixed; in plots (d, h, l),  $T$  varies, while pH<sub>rbc</sub>, either  $P_{\text{O}_2}$  or  $P_{\text{CO}_2}$ , and [DPG]<sub>rbc</sub> are fixed. In each plot, the long arrow shows the direction of the shift produced by increasing the value of the fourth variable. The shifts in the HbO<sub>2</sub> dissociation curves seen in plots (e–h) are correlated with the variations in the  $P_{50}$  values plotted in Fig. 2a–d (solid lines), as defined by Eq. 9a–d and validated by diverse experimental data in Fig. 3a–d. Similarly, the shifts in the HbCO<sub>2</sub> dissociation curves seen in plots (i–l) are correlated with the extent of CO<sub>2</sub> binding with Hb under stipulated physiological conditions, as validated by diverse experimental data in Fig. 3e–f

The accuracy and robustness of our simplified and extended models of  $S_{\text{HbO}_2}$  and  $S_{\text{HbCO}_2}$  under varying physiological conditions ( $P_{50}$  defined by Eqs. 9 and 10, and variable  $nH$  defined by Eq. 11) has also been tested against diverse experimental data available from the literature (Joels and Pugh 1958; Naeraa et al. 1963; Bauer and Schroder 1972; Hlastala et al. 1977; Matthew et al. 1977; Reeves 1980), and is illustrated in Fig. 3. Our refined  $S_{\text{HbO}_2}$  model (i.e. the simplified  $S_{\text{HbO}_2}$  model with variable  $nH$ ) is able to reproduce the  $S_{\text{HbO}_2}$  data of Joels and Pugh (1958) and Naeraa et al. (1963) obtained for a range of values of pH and  $P_{\text{CO}_2}$  at 37 °C (Fig. 3a, b) as well as the  $S_{\text{HbO}_2}$  data of Hlastala et al. (1977) and Reeves (1980) obtained over a range of values of  $T$  at fixed  $P_{\text{CO}_2}$  and pH (Fig. 3c, d). These data allow a more accurate determination of the coefficients for use in the polynomial expressions for  $P_{50,\Delta\text{pH}}$ ,  $P_{50,\Delta\text{CO}_2}$ ,  $P_{50,\Delta\text{DPG}}$ , and  $P_{50,\Delta T}$ , and hence characterize the dependence of  $P_{50}$  on pH,  $P_{\text{CO}_2}$ , [DPG] and  $T$ , and the corresponding shifts in the HbO<sub>2</sub> dissociation curves. Similarly, our refined model of  $S_{\text{HbCO}_2}$  is able to reproduce the  $S_{\text{HbCO}_2}$  data of Bauer and Schröder (1972) and Matthew et al. (1977) obtained as a function of pH<sub>rbc</sub> in oxygenated and deoxygenated blood with either constant  $P_{\text{CO}_2}$  of 40 mmHg at 37 °C (Fig. 3e) or constant total [CO<sub>2</sub>] of 55 mM at 30 °C (Fig. 3f). These model fittings provide accurate estimates of the equilibrium constants associated with the binding of CO<sub>2</sub> to oxygenated and deoxygenated Hb as well as the ionization constants of oxygenated and deoxygenated Hb at 30 and 37 °C (see Table 1). These estimates differ slightly from those used in our previous models of  $S_{\text{HbO}_2}$

and  $S_{\text{HbCO}_2}$  (Dash and Bassingthwaite 2010), but are in close agreement with those reported by Bauer and Schröder (1972) and Rossi-Bernardi and Roughton (1967). It can be noted here that the estimates of the parameters associated with the  $P_{\text{O}_2}$ -dependent variable  $nH$  for these different data sets are all similar, further signifying the importance of the variable cooperativity hypothesis in accurately simulating HbO<sub>2</sub> dissociation curves in the whole saturation range under varying physiological conditions.

Simulations of the apparent HbO<sub>2</sub> binding constant  $K'_4$ , HbO<sub>2</sub> dissociation curves, and HbCO<sub>2</sub> dissociation curves over a wide range of physiological conditions ( $P_{\text{O}_2}$ ,  $P_{\text{CO}_2}$ , pH, [DPG], and  $T$ ) are based on our refined models of  $K'_4$ ,  $S_{\text{HbO}_2}$  and  $S_{\text{HbCO}_2}$  with the  $P_{\text{O}_2}$ -dependent variable cooperativity hypothesis for O<sub>2</sub>-Hb binding, and are shown in Fig. 4. The models of  $S_{\text{HbO}_2}$  and  $S_{\text{HbCO}_2}$  simulate the Bohr and Haldane effects, and the synergistic effects of 2,3-DPG and  $T$  on the HbO<sub>2</sub> and HbCO<sub>2</sub> dissociation curves. These simulations are consistent with the previous simulations by Dash and Bassingthwaite (2010), except for their greater accuracy. The shifts in the HbO<sub>2</sub> dissociation curves seen in Fig. 4e–h are correlated with the variations in the  $P_{50}$  values plotted in Fig. 2a–d (solid lines), as defined by Eq. 9a–d and validated by diverse experimental data in Fig. 3a–d. Similarly, the shifts in the HbCO<sub>2</sub> dissociation curves seen in Fig. 4i–l are correlated with the extent of CO<sub>2</sub> binding to Hb under stipulated physiological conditions, as validated by diverse experimental data in Fig. 3e–f. These simulations clearly show the different effect of each variable on O<sub>2</sub> and CO<sub>2</sub> binding to Hb; pH is shown to significantly influence the O<sub>2</sub> and CO<sub>2</sub> binding, compared with the smaller effects of  $P_{\text{CO}_2}$ , 2,3-DPG, and  $T$ .

The accurate and efficient numerical inversion of our refined  $S_{\text{HbO}_2}$  model under standard physiological conditions is demonstrated in Fig. 5, based on the data of Severinghaus and colleagues (Roughton et al. 1972; Roughton and Severinghaus 1973; Severinghaus 1979); Winslow et al. (1977). The inset plots in Fig. 5a, b clearly show the improved agreement between the inverted  $P_{\text{O}_2}$  values and the experimental  $P_{\text{O}_2}$  values at lower  $S_{\text{HbO}_2}$  levels (<40 %) when the Hill coefficient  $nH$  is allowed to vary as a function  $P_{\text{O}_2}$  according to Eq. 11, rather than being held constant. A similar conclusion may be drawn from Fig. 5c, d. The results for the inverse problem are consistent with the results for the forward problem shown in Fig. 1. The comprehensive simulations of the numerical inversions under varying physiological conditions are shown in Fig. 6. These include the simulations of  $P_{\text{O}_2}$  as a function of  $S_{\text{HbO}_2}$  and the simulations of  $P_{\text{CO}_2}$  as a function of  $S_{\text{HbCO}_2}$  over a wide range of values of the relevant physiological variables. In each scenario, three variables are fixed at their standard physiological levels, while the fourth one is allowed to increase by predetermined increments over a large range,

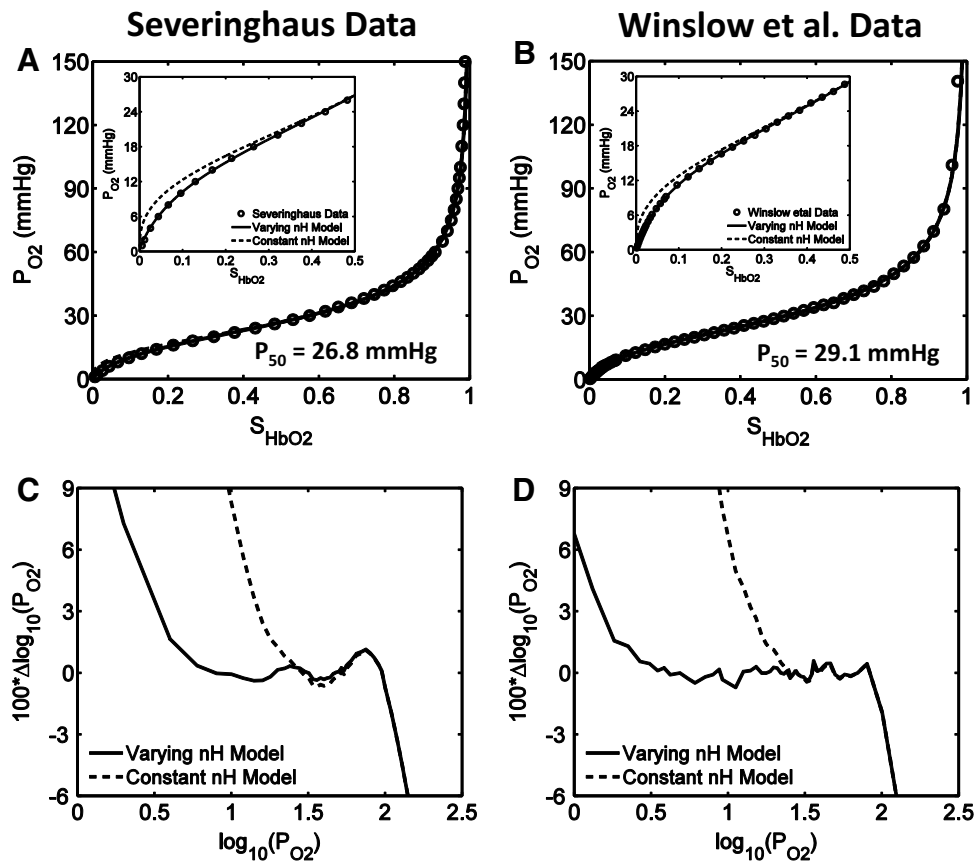


**Fig. 5** Illustration of the accurate numerical inversion of the modified  $S_{HbO_2}$  model under standard physiological conditions with the  $P_{O_2}$ -dependent variable cooperativity hypothesis for  $O_2$ -Hb binding. **a, b** Comparison of the numerically-inverted  $P_{O_2}$  values from the  $S_{HbO_2}$  values with constant and variable cooperativity hypotheses for  $O_2$ -Hb binding (constant and variable Hill coefficient  $nH$ ) to available experimental data in the literature on normal human blood at standard physiological conditions. The numerical inversions in *panel a* are compared to the data of Severinghaus and colleagues (Roughton and Severinghaus 1973; Roughton and Severinghaus 1973; Severinghaus 1979), and those in *panel b* are compared to the data of Winslow et al. (1977). The numerical inversions in the main plots are compared to the data over the whole  $S_{HbO_2}$  range, while those in the inset plots are

compared to the data for  $S_{HbO_2} \leq 0.5$ , effectively demonstrating the accurate numerical inversion of the modified  $S_{HbO_2}$  model with variable  $nH$  in simulating the data in the lower  $S_{HbO_2}$  range. **c, d** The percentage deviations  $[100 \times \Delta \log_{10}(P_{O_2})]$  of the numerically-inverted  $\log_{10}(P_{O_2})$  values from the experimental  $\log_{10}(P_{O_2})$  values for the constant and variable  $nH$  models plotted as functions of  $\log_{10}(P_{O_2})$  for the data of Severinghaus and colleagues (Roughton and Severinghaus 1973; Roughton and Severinghaus 1973; Severinghaus 1979) and Winslow et al. (1977). The  $P_{O_2}$  dependencies of  $nH$  for these two data sets are as shown in Fig. 1e, f. The incorporation of the variable cooperativity hypothesis for  $O_2$ -Hb binding (variable  $nH$ ) has improved the accuracy of the numerically-inverted  $P_{O_2}$  values from the  $S_{HbO_2}$  values

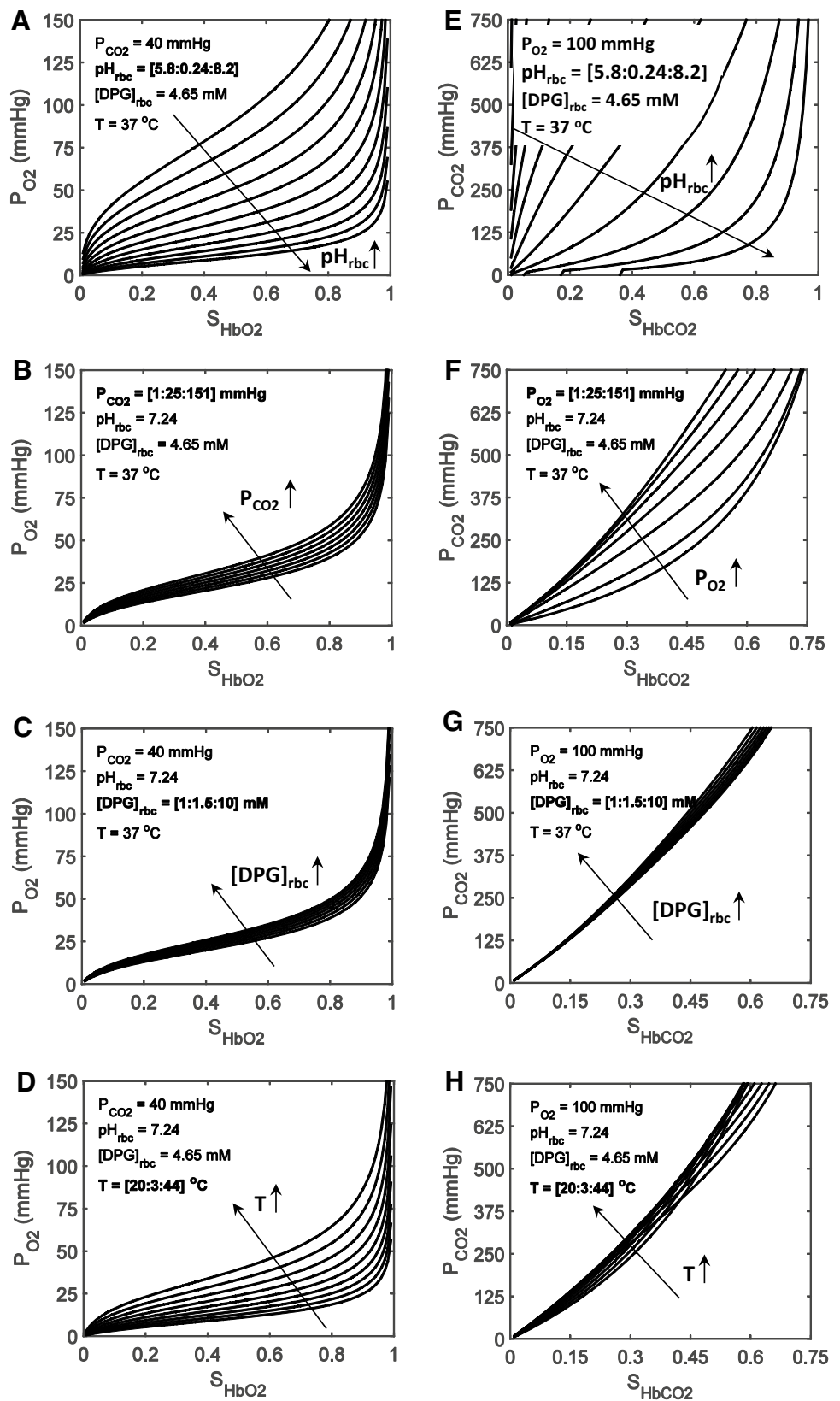
as in the simulations for the forward problem in Fig. 4. It is apparent that our iterative numerical inversion schemes are able to effectively simulate  $P_{O_2}$  and  $P_{CO_2}$  levels from the  $S_{HbO_2}$  and  $S_{HbCO_2}$  levels over a wide range of physiological conditions.

## Discussion

We have shown here how shifts in the  $HbO_2$  dissociation curve due to variations in  $P_{CO_2}$ , pH, 2,3-DPG, and  $T$  (where the variations occur in one variable at a time or several variables simultaneously) may be handled easily in the Hill equation by using an equation of state for  $P_{50}$  which

incorporates the contribution from each of these four variables. While other equations exist for  $P_{50}$ , to the best of our knowledge, none incorporates contributions from all of the four variables under discussion or is as extensively validated using independent experimental data. Moreover, we believe that Eq. 10 is the most accurate equation of state for  $P_{50}$  currently available. Although standard versions of Hill's two-parameter equation for  $S_{HbO_2}$  (using only  $P_{50}$  and  $nH$ ) have been widely used in the past, it is recognized that when  $nH$  is set equal to 2.7, as is common practice, the equation is inaccurate for  $S_{HbO_2}$  below 30 % and above 98 % (Dash and Bassingthwaite 2010), thus stimulating the development of improved descriptions by Adair (1925); Kelman (1966b); Severinghaus (1979); Siggard-Andersen

**Fig. 6** Illustration of the effective numerical inversion of our improved  $S_{HbO_2}$  and  $S_{HbCO_2}$  equations under varying physiological conditions. In plots (a–d), the simulations of  $P_{O_2}$  as a function of  $S_{HbO_2}$  are shown, while in plots (e–h), the simulations of  $P_{CO_2}$  as a function of  $S_{HbCO_2}$  are shown. In each scenario, three variables are fixed at their standard physiological levels, while the fourth one is allowed to increase by predetermined increments over a large range, as described in detail in the legend to Fig. 4. The inversion computations were carried out using a variant of the Newton–Raphson method (i.e. quasi-Newton–Raphson method) with appropriate initial guesses that guaranteed convergence. These plots are the mirror images of the corresponding plots in Fig. 4 (but with different scales), illustrating the accuracy of the numerical inversion schemes



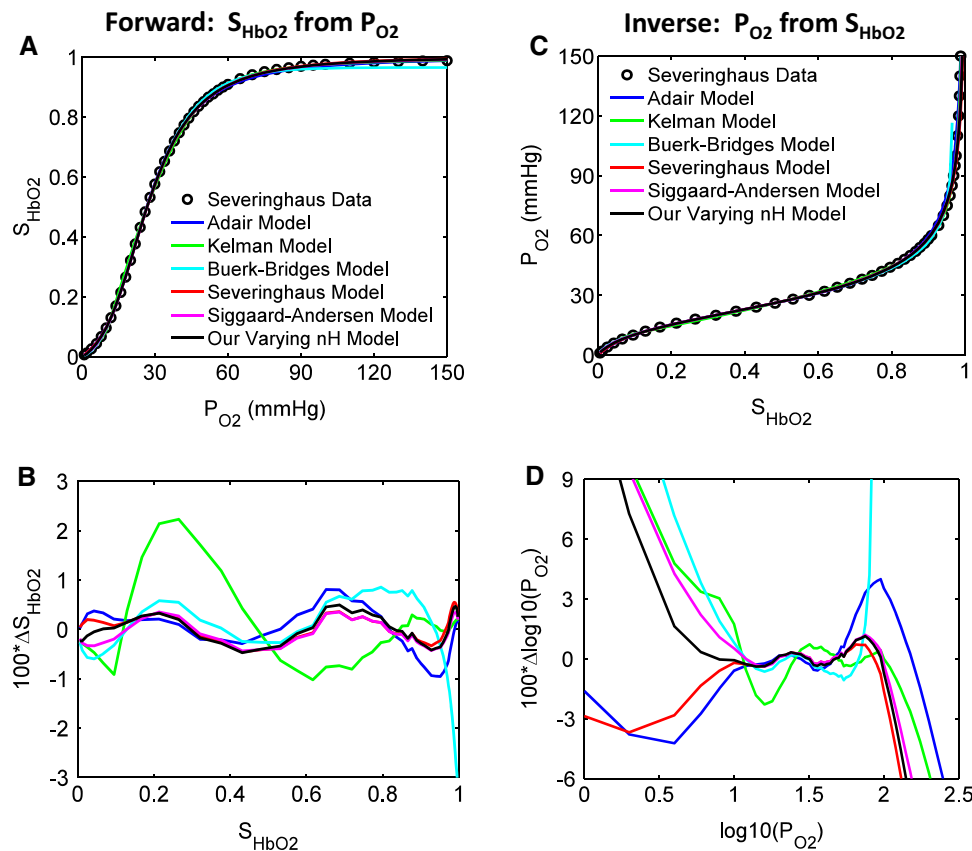


**Fig. 7** Comparison of our improved  $S_{\text{HbO}_2}$  model with alternative  $S_{\text{HbO}_2}$  models from the literature in simulating available experimental data at standard physiological conditions (both forward and inverse problems). In each case, the model for comparison has first been parameterized to produce a “best fit” based on the experimental data. **a** HbO<sub>2</sub> dissociation curves obtained from our improved  $S_{\text{HbO}_2}$  model compared with those obtained from other commonly used  $S_{\text{HbO}_2}$  models (Adair 1925; Kelman 1966b; Severinghaus 1979; Siggaard-Andersen et al. 1984; Buerk and Bridges 1986), in simulating the data of Severinghaus and colleagues (Roughton and Severinghaus 1973; Roughton and Severinghaus 1973; Severinghaus 1979) on normal human blood at standard physiological conditions. **b** The percentage deviations ( $100 \times \Delta S_{\text{HbO}_2}$ ) of the model-simulated  $S_{\text{HbO}_2}$  values from the experimental  $S_{\text{HbO}_2}$  values based on our improved  $S_{\text{HbO}_2}$  model and the alternative models, plotted as functions of  $S_{\text{HbO}_2}$  for the data of Severinghaus and colleagues (Roughton and Severinghaus

1973; Roughton and Severinghaus 1973; Severinghaus 1979). **c** Comparisons of the numerically-inverted  $P_{\text{O}_2}$  values from the  $S_{\text{HbO}_2}$  values obtained from our improved  $S_{\text{HbO}_2}$  model and the alternative models, in simulating the data of Severinghaus and colleagues (Roughton and Severinghaus 1973; Roughton and Severinghaus 1973; Severinghaus 1979) on normal human blood at standard physiological conditions. **d** The percentage deviations [ $100 \times \Delta \log_{10}(P_{\text{O}_2})$ ] of the numerically-inverted  $\log_{10}(P_{\text{O}_2})$  values from the experimental  $\log_{10}(P_{\text{O}_2})$  values based on our improved  $S_{\text{HbO}_2}$  model and the alternative  $S_{\text{HbO}_2}$  models, plotted as functions of  $\log_{10}(P_{\text{O}_2})$  for the data of Severinghaus and colleagues (Roughton and Severinghaus 1973; Roughton and Severinghaus, 1973; Severinghaus 1979). The comparison may be repeated using the data of Winslow et al. (1977). This involves the re-parameterization of each model to obtain the best fit to the data. The result has not been shown here as it does not contribute anything further to the conclusions already drawn

et al. (1984); Buerk and Bridges (1986), and others. In this paper, we have addressed this important deficiency in the standard Hill equation by expressing the Hill coefficient  $nH$  as a simple exponential function of  $P_{\text{O}_2}$  (Eq. 11), with  $P_{50}$  given by Eq. 10. Figures 1, 3, and 5 show that this change improves the agreement between the model and available experimental data at both standard physiological conditions and at other values of pH,  $P_{\text{CO}_2}$ , 2,3-DPG, and temperature that characterize pathophysiological states.

So the question that arises is this: Using these modifications, how does Hill’s equation compare with other

commonly used mathematical models of the HbO<sub>2</sub> dissociation curve? In Fig. 7a, c, we show the fit of our new refined Hill-based equation for  $S_{\text{HbO}_2}$  to the data of Severinghaus and colleagues (Roughton et al. 1972; Roughton and Severinghaus 1973; Severinghaus 1979) under standard physiological conditions and compare that to the fit obtained using the  $S_{\text{HbO}_2}$  models of Adair (1925), Kelman (1967), Buerk and Bridges (1986), Severinghaus (1979), and Siggaard-Andersen et al. (1984, 1990) for both the forward (computation of  $S_{\text{HbO}_2}$  from  $P_{\text{O}_2}$ ) and inverse (computation of  $P_{\text{O}_2}$  from  $S_{\text{HbO}_2}$ ) situations. The associated residual errors

are shown in Fig. 7b, d. Although all the models shown in Fig. 7a seem to provide a good fit to the data (except for Kelman (1966b) for some  $P_{O_2}$  values and Buerk and Bridges (1986) for high  $P_{O_2}$ ), the residual error shown in Fig. 7b is least for our present model and the models of Severinghaus (1979) and Siggaard-Andersen et al. (1984, 1990). Figure 7c shows that all the models also produce a good fit to the data of Severinghaus and colleagues (Roughton et al. 1972; Roughton and Severinghaus 1973; Severinghaus 1979) on inversion, but the error plotted in Fig. 7d indicates that our model is the most accurate for  $P_{O_2}$  greater than  $10^{0.5}$  (i.e.  $P_{O_2} > 3$ ) mmHg. Note that the distinction between the various models for the inverse problem is more apparent because of the use of a log–log scale. Apart from the two exceptions mentioned above, when compared with the data most of these models provide accuracy greater than 99.5 % over the whole saturation range.

We also note here that the other  $S_{HbO_2}$  models shown in Fig. 7 were parameterized based on the data of Severinghaus and colleagues (Roughton et al. 1972; Roughton and Severinghaus 1973; Severinghaus 1979), and hence a comparison of the models with respect to the data of Winslow et al. (1977) cannot be made, unless they are re-parameterized. This is not the purpose of Fig. 7. Rather, the purpose of Fig. 7 is to illustrate how our new refined  $S_{HbO_2}$  model is “at least” comparable in terms of accuracy to many other  $S_{HbO_2}$  models used widely in the literature. Figure 7 shows that this is indeed the case, yet our model is simpler than many others and efficiently invertible.

The recent model of Matejak et al. (2015), based on their version of the Adair equation (1925), is reported to fit well, the data of Severinghaus and colleagues (Roughton et al. 1972; Roughton and Severinghaus 1973; Severinghaus 1979), and is also shown to fit the temperature and pH-dependent  $S_{HbO_2}$  data of Reeves (1980) and Naeraa (1963), and carbaminohemoglobin data of Bauer and Schröder (1972) and Matthew (1977). Our present  $S_{HbO_2}$  and  $S_{HbCO_2}$  models fit these diverse data sets as accurately, and also fit the  $P_{CO_2}$ , pH, and temperature-dependent data of Joels and Pugh (1958) and Hlastala et al. (1977), which were not used by Matejak et al. (2015). Thus, the present  $S_{HbO_2}$  and  $S_{HbCO_2}$  models are well-validated based on a larger set of experimental data. More importantly, not only is our new refined  $S_{HbO_2}$  model more accurate over the whole saturation range (important for the integrated computational modeling of alveolar-blood and blood-tissue  $O_2$ – $CO_2$  transport, exchange, and metabolism), it is also much simpler than our previous  $S_{HbO_2}$  model, as there is no need to perform the complex computations to derive the indices  $n_1$ ,  $n_2$ ,  $n_3$ , and  $n_4$ .

The  $HbCO_2$  dissociation curve is obtained in our treatment from Eq. 1b. The expression for  $K_{HbCO_2}$  is derived from Eqs. 3b and 4. When  $S_{HbO_2}$  equals 1,  $K_{HbCO_2}$  equals  $K'_3\Phi_2/\Phi_4$ . Otherwise  $K'_4$  is required and is given by Eq. 7.

Fortuitously, all the information regarding the variables  $P_{CO_2}$ , pH, 2,3-DPG and  $T$  is contained in Eq. 10, the equation of state for  $P_{50}$ . Thus, in our treatment, both  $S_{HbO_2}$  and  $S_{HbCO_2}$  rely on this equation for information about  $P_{CO_2}$ , pH, 2,3-DPG and  $T$ . Other authors incorporate this information in different ways. For example, Severinghaus (1979) provides one equation for the temperature coefficient of  $P_{O_2}$  and another for the change in  $\ln P_{O_2}$  per unit change in pH. If instead of equating Eq. 6 with Eq. 1a, we equate the Severinghaus equation for  $S_{HbO_2}$  with Eq. 1a, we obtain the following expression for  $K'_4$ :

$$K'_4 = \frac{(150 + 23400P_{O_2}^2)(K'_2\alpha_{CO_2}P_{CO_2}\Phi_1 + \Phi_3)}{\alpha_{O_2}(K'_3\alpha_{CO_2}P_{CO_2}\Phi_2 + \Phi_4)} \quad (12)$$

The value for  $P_{O_2}$  used in Eq. 12 is that obtained after correction for temperature and pH. A similar approach may be adopted in the case of the Adair equation (Adair 1925) to transfer information regarding pH, 2,3-DPG and  $T$  to the  $CO_2$ -Hb reaction system. Thus, Eq. 1b can be adapted for use with a variety of models of the  $HbO_2$  dissociation curve.

Inversion of  $S_{HbO_2}$  and  $S_{HbCO_2}$  equations is an essential feature in modeling of alveolar-blood and blood-tissue  $O_2$ – $CO_2$  exchange at a sophisticated level. Algebraic inversion is possible with the Severinghaus  $S_{HbO_2}$  Eq. (1979), but not in our models, once the Hill coefficient  $nH$  is allowed to vary. Iterative approaches are generally used for this. The Appendix provides fixed-point and quasi-Newton–Raphson iterative methods that would also be applicable to the models of Matejak et al. (2015) and others that are not analytically invertible.

## Conclusions

We have simplified and extended our previously developed mathematical models of blood  $HbO_2$  and  $HbCO_2$  dissociation curves (Dash and Bassingthwaite 2010) to make them accurate over the whole saturation range for a wide range of values of  $P_{O_2}$ ,  $P_{CO_2}$ , pH, 2,3-DPG, and temperature. The extended  $S_{HbO_2}$  model features a  $P_{O_2}$ -dependent variable Hill coefficient  $nH$  for the binding of  $O_2$  to Hb, and incorporates a modified  $P_{50}$  model that provides accurate shifts in the  $HbO_2$  dissociation curve over a wide range of physiological conditions, validated by diverse experimental data sets available in the literature. The information contained in this modified equation for  $P_{50}$  is transferred to the  $HbCO_2$  dissociation curve via  $K'_4$ , the apparent equilibrium constant in a single-step binding reaction of  $O_2$  and Hb. The coupling of the Hb dissociation curves for  $O_2$  and  $CO_2$  may also be accomplished using models of  $S_{HbO_2}$  other than the Hill equation. Finally, the extended  $S_{HbO_2}$  and  $S_{HbCO_2}$  models are conveniently

invertible for efficient computation of  $P_{O_2}$  from  $S_{HbO_2}$  and  $P_{CO_2}$  from  $S_{HbCO_2}$ , using simple iterative numerical schemes with appropriate starting values that guarantee convergence. The calculations involved in our new  $S_{HbO_2}$  and  $S_{HbCO_2}$  models may be performed on handheld devices. More importantly, they can conveniently be used in the integrated computational modeling of alveolar-blood and blood-tissue  $O_2$ – $CO_2$  transport, exchange, and metabolism for analysis and mechanistic understanding of in vitro and in vivo blood gas data under physiological and non-physiological conditions, such as ischemia and reperfusion, extremes in gas concentrations, high altitudes, and extreme temperatures.

**Acknowledgments** We thank the reviewers for helpful and insightful comments that have enhanced the overall quality of the manuscript. This work was supported by the National Institute of Health Grants P50-GM094503 and P01-GM066730. The extension of  $P_{50}$  model to extreme/wider physiological conditions (e.g. pH > 8.5) was motivated by RKD's email correspondence with Stefan Kleiser (University Hospital Zurich), a user of the 2010 Dash and Bassingthwaite  $S_{HbO_2}$  and  $S_{HbCO_2}$  models.

### Appendix: Efficient iterative schemes for numerical computations of $P_{O_2}$ from $S_{HbO_2}$ and $P_{CO_2}$ from $S_{HbCO_2}$

Two efficient numerical methods are presented below for the inversion of  $P_{O_2}$  from  $S_{HbO_2}$  and  $P_{CO_2}$  from  $S_{HbCO_2}$ , based on fixed-point and quasi-Newton–Raphson iteration methods (Scheme-1 and Scheme-2, respectively) (Heath 2002; Pozrikidis 2008).

The iterative schemes for the computation of  $P_{O_2}$  from  $S_{HbO_2}$  are given by:

Scheme-1:

$$P_{O_2}^{New} = P_{50} \left( \frac{S_{HbO_2}^{Input}}{1 - S_{HbO_2}^{Input}} \right)^{\frac{1}{nH(P_{O_2}^{Old})}} \quad (A-1a)$$

Scheme-2:

$$\begin{aligned} P_{O_2}^{New} &= P_{O_2}^{Old} - \left( \frac{S_{HbO_2}(P_{O_2}^{Old}) - S_{HbO_2}^{Input}}{S'_{HbO_2}(P_{O_2}^{Old})} \right) \\ &= P_{O_2}^{Old} - \left( \frac{0.02P_{O_2}^{Old} (S_{HbO_2}(P_{O_2}^{Old}) - S_{HbO_2}^{Input})}{S_{HbO_2}(P_{O_2}^{Old} + 0.01P_{O_2}^{Old}) - S_{HbO_2}(P_{O_2}^{Old} - 0.01P_{O_2}^{Old})} \right) \end{aligned} \quad (A-1b)$$

where  $S_{HbO_2}^{Input}$  is the input  $S_{HbO_2}$  (given),  $S_{HbO_2}(P_{O_2}^{Old})$  is the value of  $S_{HbO_2}$  evaluated at  $P_{O_2}^{Old}$ , and  $S'_{HbO_2}(P_{O_2}^{Old})$  is the derivative of  $S_{HbO_2}$  w.r.t.  $P_{O_2}$  evaluated at  $P_{O_2}^{Old}$ . Either Eq. 1a or Eq. 6 can be used as the expression for  $S_{HbO_2}$ .

In the second version of Eq. A-1b, it is only necessary to perform function evaluation, because  $S'_{HbO_2}(P_{O_2}^{Old})$  has been estimated using a central-difference formula for first-order derivatives (Pozrikidis 2008), which eliminates the need to differentiate the expression for  $S_{HbO_2}$ , which may be complicated. If the Hill coefficient  $nH$  is held constant, Eq. A-1a itself provides the analytical inversion for the computation of  $P_{O_2}$  from  $S_{HbO_2}$ . For  $P_{O_2}$ -dependent  $nH$  (Eq. 11), the iteration scheme of Eq. A-1a converges within 3 to 5 iterations with  $10^{-3}$  accuracy, using any starting value for  $P_{O_2}$ . For the same accuracy, the iteration scheme of Eq. A-1b converges within 5–8 iterations using  $P_{50}$  from Eq. 10 as the starting value for  $P_{O_2}$ .

The analogous iterative schemes for the computation of  $P_{CO_2}$  from  $S_{HbCO_2}$  are given by:

Scheme-1:

$$P_{CO_2}^{New} = \left( \frac{S_{HbCO_2}^{Input}}{1 - S_{HbCO_2}^{Input}} \right) \left( \frac{1}{\alpha_{CO_2} K_{HbCO_2} (P_{CO_2}^{Old})} \right) \quad (A-2a)$$

Scheme-2:

$$\begin{aligned} P_{CO_2}^{New} &= P_{CO_2}^{Old} - \left( \frac{S_{HbCO_2}(P_{CO_2}^{Old}) - S_{HbCO_2}^{Input}}{S'_{HbCO_2}(P_{CO_2}^{Old})} \right) \\ &= P_{CO_2}^{Old} - \left( \frac{0.02P_{CO_2}^{Old} (S_{HbCO_2}(P_{CO_2}^{Old}) - S_{HbCO_2}^{Input})}{S_{HbCO_2}(P_{CO_2}^{Old} + 0.01P_{CO_2}^{Old}) - S_{HbCO_2}(P_{CO_2}^{Old} - 0.01P_{CO_2}^{Old})} \right) \end{aligned} \quad (A-2b)$$

Similar iterative methods can be used to compute  $P_{O_2}$  from total  $[O_2]$  and  $P_{CO_2}$  from total  $[CO_2]$ . Note that the total  $[O_2]$  and the total  $[CO_2]$  are defined in Table 1.

### References

- Adair GS (1925) The hemoglobin system VI. The oxygen dissociation curve of hemoglobin. *J Biol Chem* 63:529–545
- Austin WH, Lacombe E, Rand PW, Chatterjee M (1963) Solubility of carbon dioxide in serum from 15 to 38 C. *J Appl Physiol* 18:301–304
- Bassingthwaite JB, Beard DA, Carlson BE, Dash RK, Vinnakota K (2012) Modeling to link regional myocardial work, metabolism and blood flows. *Ann Biomed Eng* 40:2379–2398
- Bauer C, Schroder E (1972) Carbamino compounds of haemoglobin in human adult and foetal blood. *J Physiol* 227:457–471
- Buerk DG, Bridges EW (1986) A simplified algorithm for computing the variation in oxyhemoglobin saturation with pH,  $PCO_2$ , T and DPG. *Chem Eng Commun* 47:113–124
- Dash RK, Bassingthwaite JB (2004) Blood  $HbO_2$  and  $HbCO_2$  dissociation curves at varied  $O_2$ ,  $CO_2$ , pH, 2,3-DPG and temperature levels. *Ann Biomed Eng* 32:1676–1693
- Dash RK, Bassingthwaite JB (2006) Simultaneous blood-tissue exchange of oxygen, carbon dioxide, bicarbonate, and hydrogen ion. *Ann Biomed Eng* 34:1129–1148



- Dash RK, Bassingthwaite JB (2010) Erratum to: blood HbO<sub>2</sub> and HbCO<sub>2</sub> dissociation curves at varied O<sub>2</sub>, CO<sub>2</sub>, pH, 2,3-DPG and temperature levels. *Ann Biomed Eng* 38:1683–1701
- Forster RE, Constantine HP, Craw MR, Rotman HH, Klocke RA (1968) Reaction of CO<sub>2</sub> with human hemoglobin solution. *J Biol Chem* 243:3317–3326
- Geers C, Gros G (2000) Carbon dioxide transport and carbonic anhydrase in blood and muscle. *Physiol Rev* 80:681–715
- Heath MT (2002) Scientific computing: an introductory survey. The McGraw-Hill Companies Inc, Boston
- Hedley-Whyte J, Laver MB (1964) O<sub>2</sub> Solubility in Blood and Temperature Correction Factors for P<sub>O<sub>2</sub></sub>. *J Appl Physiol* 19:901–906
- Hlastala MP, Woodson RD, Wranne B (1977) Influence of temperature on hemoglobin-ligand interaction in whole blood. *J Appl Physiol Respir Environ Exerc Physiol* 43:545–550
- Joels N, Pugh LG (1958) The carbon monoxide dissociation curve of human blood. *The Journal of Physiology* 142:63–77
- Kelman GR (1966a) Calculation of certain indices of cardio-pulmonary function, using a digital computer. *Respir Physiol* 1:335–343
- Kelman GR (1966b) Digital computer subroutine for the conversion of oxygen tension into saturation. *J Appl Physiol* 21:1375–1376
- Kelman GR (1967) Digital computer procedure for the conversion of PCO<sub>2</sub> into blood CO<sub>2</sub> content. *Respir Physiol* 3:111–115
- Mateják M, Kulhanek T, Matousek S (2015) Adair-based hemoglobin equilibrium with oxygen, carbon dioxide and hydrogen ion activity. *Scand J Clin Lab Invest* 75:113–120
- Matthew JB, Morrow JS, Wittebort RJ, Gurd FR (1977) Quantitative determination of carbamino adducts of alpha and beta chains in human adult hemoglobin in presence and absence of carbon monoxide and 2,3-diphosphoglycerate. *J Biol Chem* 252:2234–2244
- Naeraa N, Petersen ES, Boye E (1963) The influence of simultaneous, independent changes in pH and carbon dioxide tension on the in vitro oxygen tension-saturation relationship of human blood. *Scand J Clin Lab Invest* 15:141–151
- Pozrikidis C (2008) Numerical computations in science and engineering. Oxford University Press, New York
- Rees SE, Andreassen S (2005) Mathematical models of oxygen and carbon dioxide storage and transport: the acid-base chemistry of blood. *Crit Rev Biomed Eng* 33:209–264
- Reeves RB (1980) The effect of temperature on the oxygen equilibrium curve of human blood. *Respir Physiol* 42:317–328
- Rossi-Bernardi L, Roughton FJ (1967) The specific influence of carbon dioxide and carbamate compounds on the buffer power and Bohr effects in human haemoglobin solutions. *J Physiol* 189:1–29
- Roughton FJW, Deland EC, Kernohan JC, Severinghaus JW (1972) Some recent studies of the oxyhemoglobin dissociation curve of human blood under physiological conditions and the fitting of the Adair equation to the standard curve. In: Rørth M, Astrup P (eds) Proceedings of the oxygen affinity of hemoglobin and red cell acid base status, proceedings of the alfred benzon symposium IV held at the premises of the royal danish academy of sciences and letters, pp 73–81
- Roughton FJ, Severinghaus JW (1973) Accurate determination of O<sub>2</sub> dissociation curve of human blood above 98.7 percent saturation with data on O<sub>2</sub> solubility in unmodified human blood from 0 degrees to 37 degrees C. *J Appl Physiol* 35:861–869
- Severinghaus JW (1979) Simple, accurate equations for human blood O<sub>2</sub> dissociation computations. *J Appl Physiol Respir Environ Exerc Physiol* 46:599–602
- Siggaard-Andersen O (1971) Oxygen-linked hydrogen ion binding of human hemoglobin. Effects of carbon dioxide and 2,3-diphosphoglycerate. I. Studies on erythrolysate. *Scand J Clin Lab Invest* 27:351–360
- Siggaard-Andersen O, Garby L (1973) The Bohr effect and the Haldane effect. *Scand J Clin Lab Invest* 31:1–8
- Siggaard-Andersen O, Salling N (1971) Oxygen-linked hydrogen ion binding of human hemoglobin. Effects of carbon dioxide and 2,3-diphosphoglycerate. II. Studies on whole blood. *Scand J Clin Lab Invest* 27:361–366
- Siggaard-Andersen O, Siggaard-Andersen M (1990) The oxygen status algorithm: a computer program for calculating and displaying pH and blood gas data. *Scand J Clin Lab Invest Suppl* 203:29–45
- Siggaard-Andersen O, Rørth M, Norgaard-Pedersen B, Andersen OS, Johansen E (1972a) Oxygen-linked hydrogen ion binding of human hemoglobin. Effects of carbon dioxide and 2,3-diphosphoglycerate. IV. Thermodynamical relationship between the variables. *Scand J Clin Lab Invest* 29:303–320
- Siggaard-Andersen O, Salling N, Norgaard-Pedersen B, Rørth M (1972b) Oxygen-linked hydrogen ion binding of human hemoglobin. Effects of carbon dioxide and 2,3-diphosphoglycerate. *Scand J Clin Lab Invest* 29:185–193
- Siggaard-Andersen O, Wimberley PD, Gothgen I, Siggaard-Andersen M (1984) A mathematical model of the hemoglobin-oxygen dissociation curve of human blood and of the oxygen partial pressure as a function of temperature. *Clin Chem* 30:1646–1651
- Tyuma I (1984) The Bohr effect and the Haldane effect in human hemoglobin. *Jpn J Physiol* 34:205–216
- von Restorff W, Holtz J, Bassenge E (1977) Exercise induced augmentation of myocardial oxygen extraction in spite of normal coronary dilatatory capacity in dogs. *Pflugers Arch* 372:181–185
- Winslow RM, Swenberg ML, Berger RL, Shrager RI, Luzzana M, Samaja M, Rossi-Bernardi L (1977) Oxygen equilibrium curve of normal human blood and its evaluation by Adair's equation. *J Biol Chem* 252:2331–2337
- Winslow RM, Samaja M, Winslow NJ, Rossi-Bernardi L, Shrager RI (1983) Simulation of continuous blood O<sub>2</sub> equilibrium curve over physiological pH, DPG, and PCO<sub>2</sub> range. *J Appl Physiol Respir Environ Exerc Physiol* 54:524–529
- Wolf MB (2013) Whole body acid-base and fluid-electrolyte balance: a mathematical model. *Am J Physiol Renal Physiol* 305:F1118–F1131